Molecular Pharmacology Fast Forward. Published on July 25, 2016 as DOI: 10.1124/mol.116.104919
This article has not been copyedited and formatted. The final version may differ from this version.

WNT stimulation dissociates a Frizzled 4 inactive state complex with $G\alpha_{12/13}$

Elisa Arthofer, Belma Hot, Julian Petersen, Katerina Strakova, Stefan Jäger, Manuel Grundmann, Evi Kostenis, J. Silvio Gutkind, Gunnar Schulte

Section of Receptor Biology & Signaling, Dept. Physiology & Pharmacology, Karolinska Institutet, S-17177, Stockholm, Sweden (EA, BH, JP, KS, SJ, GS)

Section on Molecular Signal Transduction Eunice Kennedy Shriver National Institute of Child Health and Human Development, National Institutes of Health, 35A Convent Drive, MSC 3752 Bethesda, MD 20892-3752, USA. (EA)

Faculty of Science, Institute of Experimental Biology, Masaryk University, Brno, Czech Republic (KS, GS)

Molecular-, Cellular- and Pharmacobiology Section, Institute for Pharmaceutical Biology, University of Bonn, 53115 Bonn, Germany (MG, EK)

University of California San Diego, Dept. Pharmacology, Moores Cancer Center, 9500 Gilman Dr., La Jolla, CA 92093-0636, USA (JSG)

Molecular Pharmacology Fast Forward. Published on July 25, 2016 as DOI: 10.1124/mol.116.104919
This article has not been copyedited and formatted. The final version may differ from this version.

Running title: FZD_4 signaling via $G\alpha_{12/13}$ to p115-RHOGEF

Corresponding author:
Gunnar Schulte, PhD
Karolinska Institutet
Dept. Physiology & Pharmacology
Sec. Receptor Biology & Signaling
Nanna Svartz väg 2
S-171 77 Stockholm
e-mail: gunnar.schulte@ki.se
phone: +46-852487933

Number of

Text pages: 36
Tables: 0
Figures: 9
References: 71

Words in

abstract: 238
introduction: 708
discussion: 1090

List of non/standard abbreviations

dcFRAP, double color fluorescence recovery after photobleaching; DKK1, dickkopf 1; DMR, dynamic mass redistribution; DVL, disheveled; FRET, Förster resonance energy transfer; FZD, Frizzled; GAP, GTPase activating protein; GEF, guanine nucleotide exchange factor; GPCR, G protein-coupled receptor; LRP5/6, low-density lipid receptor related protein 5/6; p115-RHOGEF, RHO guanine nucleotide exchange factor, molecular weight 115 kDa; PCP, planar cell polarity; RGS, regulator or G protein signaling; WNT, Wingless/Int-1 lipoglycoproteins.

Molecular Pharmacology Fast Forward. Published on July 25, 2016 as DOI: 10.1124/mol.116.104919
This article has not been copyedited and formatted. The final version may differ from this version.

Abstract:

Frizzleds are unconventional G protein-coupled receptors (GPCRs) that belong to the Class Frizzled. They are bound and activated by the WNT family of secreted lipoglycoproteins. To date, mechanisms of signal initiation and FZD-G protein coupling remain poorly understood. Previously, we showed that FZD_6 assembles with $G\alpha_{i1}/G\alpha_q$, but not with $G\alpha_s$, $G\alpha_o$, and $G\alpha_{12/13}$ and that these inactive-state complexes are dissociated by WNTs and regulated by the phosphoprotein Dishevelled (DVL). Here, we investigated the inactive state assembly of heterotrimeric G proteins with FZD_4, a receptor important in retinal vascular development and frequently mutated in Norrie disease or familial exudative vitreoretinopathy (FEVR). Live cell imaging experiments employing fluorescence recovery after photobleaching (FRAP) show that human FZD_4 assembles – in a DVL-independent manner – with $G\alpha_{12/13}$ but not representatives of other heterotrimeric G protein subfamilies, such as $G\alpha_{i1}$, $G\alpha_o$, $G\alpha_s$ and $G\alpha_q$. The FZD_4-G protein complex dissociates upon stimulation with WNT-3A, WNT-5A, WNT-7A, and WNT-10B. In addition, WNT-induced dynamic mass redistribution (DMR) changes in untransfected and – even more so – in FZD_4-GFP transfected cells depend on $G\alpha_{12/13}$. Furthermore, expression of FZD_4 and $G\alpha_{12}$ or $G\alpha_{13}$ in HEK293 cells induces WNT-dependent membrane recruitment of p115-RHOGEF, a direct target of $G\alpha_{12/13}$ signaling, underlining the functionality of a FZD_4-$G\alpha_{12/13}$-RHO signaling axis. In summary, $G\alpha_{12/13}$-mediated WNT/FZD_4 signaling through p115-RHOGEF offers an intriguing and previously unappreciated mechanistic link of FZD_4 signaling to cytoskeletal rearrangements and RHO signaling with implications for the regulation of angiogenesis during embryonic and tumor development.

Molecular Pharmacology Fast Forward. Published on July 25, 2016 as DOI: 10.1124/mol.116.104919
This article has not been copyedited and formatted. The final version may differ from this version.

Molecular Pharmacology Fast Forward. Published on July 25, 2016 as DOI: 10.1124/mol.116.104919
This article has not been copyedited and formatted. The final version may differ from this version.

Introduction:

Wingless/Int-1 (WNT)-Frizzled (FZD) signaling is initiated through the interaction of Class Frizzled (FZD_{1-10}) receptors and their ligands of the WNT family of lipoglycoproteins. WNT signaling holds a central role in embryonic development and the development of human diseases by orchestrating a variety of cellular signaling pathways. The precise mechanisms of signal initiation and specification through WNT binding to the extracellular part of FZD and downstream signal transduction through intracellular signaling partners are so far poorly understood (Angers and Moon, 2009; Dijksterhuis et al., 2014; Nusse, 2003; Schulte, 2010; Schulte, 2015; van Amerongen and Nusse, 2009).

WNT signaling was historically divided into β-catenin-dependent and -independent pathways. β-catenin-dependent signals are initiated by WNT binding to FZD and low density lipoprotein receptor related protein 5/6 (LRP5/6), recruitment of Dishevelled (DVL) and subsequent inhibition of a destruction complex resulting in elevated β-catenin levels initiating WNT-target gene transcription (Clevers and Nusse, 2012; He et al., 2004; Macdonald et al., 2007; Tamai et al., 2000; Wehrli et al., 2000). Several β-catenin-independent signaling cascades have been described, involving small GTPases, such as RHO, RAC and Cdc42 as well as heterotrimeric G protein signaling through intracellular mobilization of calcium (Schulte, 2010; Semenov et al., 2007). These pathways regulate, for example, cell movement, cytoskeletal reorganization, and planar cell polarity (PCP)-like signaling in mammalian systems.

Accumulating mechanistic insight strengthens the concept that FZDs behave as bona fide GPCRs (Ahumada et al., 2002; Aznar et al., 2015; Halleskog et al., 2012; Katanaev and Buestorf, 2009; Katanaev et al., 2005; Kilander et al., 2014a; Kilander et al., 2014b; Kilander et al., 2011; Koval and Katanaev, 2011; Liu et al., 1999; Sheldahl et al., 1999; Slusarski et al., 1997) whereas other aspects, such as G protein coupling selectivity,

Molecular Pharmacology Fast Forward. Published on July 25, 2016 as DOI: 10.1124/mol.116.104919
This article has not been copyedited and formatted. The final version may differ from this version.

ligand-dependent functional selectivity and the importance of G protein signaling downstream of FZDs still remain obscure (Dijksterhuis et al., 2015).

Heterotrimeric G proteins interact with GPCRs according to distinct dynamic concepts: On one hand, G proteins and receptors assemble in an inactive state, which would explain receptor–G protein selectivity and the rapid responses observed in cells (Oldham and Hamm, 2008). On the other hand, random collision coupling of G protein and receptors is sufficient to form the fully active, agonist-bound receptor conformation inducing release of GDP from Gα and subsequently a rapid GTP-dependent dissociation of the receptor-G protein complex (Ayoub et al., 2012; Hein et al., 2005; Neubig, 1994; Oldham and Hamm, 2008; Rasmussen et al., 2011); both proposed scenarios are supported experimentally (Gales et al., 2005; Gales et al., 2006; Hein et al., 2005; Nobles et al., 2005; Qin et al., 2011). FZD_6 exists in an inactive state complex with heterotrimeric $G\alpha_i$ and $G\alpha_q$ (Kilander et al., 2014b) similar to what was observed for the muscarinic M_3 receptor (Qin et al., 2011). Agonist stimulation of the FZD_6-G protein complex is followed by rapid dissociation (Kilander et al., 2014b). The FZD isoform in focus in this study, FZD_4, has so far not been connected to signaling through heterotrimeric G proteins. FZD_4 signaling, especially in the physiological context of retinal vascularization, familial exudative vitreoretinopathy (FEVR) and Norrie disease, is firmly associated with WNT/β-catenin signaling depending on ligand-induced recruitment of LRP5/6 to FZD_4 (Robitaille et al., 2002; Shastry, 2010; Toomes et al., 2005; Warden et al., 2007; Xu et al., 2004). Moreover, it is intriguing that vascularization and angiogenesis, not only limited to retina, are directly but independently of each other linked to FZD_4 and G protein signaling through $G\alpha_{12/13}$/RHO signaling (Offermanns et al., 1997; Robitaille et al., 2002; Sivaraj et al., 2013; Ye et al., 2009) suggesting a biologically relevant liaison.

Molecular Pharmacology Fast Forward. Published on July 25, 2016 as DOI: 10.1124/mol.116.104919
This article has not been copyedited and formatted. The final version may differ from this version.

In this study we set out to investigate the ability of FZD_4 to mediate heterotrimeric G protein signaling. Based on live cell imaging experiments we establish that FZD_4 assembles with heterotrimeric $G\alpha_{12}$ and $G\alpha_{13}$, independently of DVL. Stimulation of FZD_4 with WNTs dissociates the receptor-G protein complex, likely leading to G protein activation and subsequent downstream signaling events. We further show that FZD_4 mediates DMR and membrane recruitment of p115-RHOGEF, a direct downstream target of active $G\alpha_{12/13}$, in a $G\alpha_{12/13}$- and WNT-dependent manner. Thus, on the basis of our results we propose a novel WNT-FZD_4-$G\alpha_{12/13}$-RHO signaling axis offering deeper mechanistic insight into FZD_4 signaling to cytoskeletal rearrangements, RHO signaling and potentially angiogenesis.

Molecular Pharmacology Fast Forward. Published on July 25, 2016 as DOI: 10.1124/mol.116.104919
This article has not been copyedited and formatted. The final version may differ from this version.

Materials and Methods

Cell Culture and Transfections

HEK293T cells (ATCC, USA) were cultured in DMEM supplemented with 10% FBS, 1% Penicillin/StreptoMYCin, 1% L-glutamine (all from Invitrogen, USA) in a humidified CO_2 incubator at 37°C. Cell culture plastics were from Sarstedt (Germany) or Corning (USA) unless otherwise specified. For live-cell imaging, immunochemical, and immunoblot analyses, cells were seeded on 35 mm Poly-L-Lysine- or matrigel (1:300 in starvation medium)-coated (Sigma-Aldrich, Sweden) glass-bottom dishes (4 chamber 35 mm glass-bottom dishes; Greiner Bio One, Germany). Cells were transfected with Lipofectamine 2000 or 3000 according to manufacturer's instructions (Life Technologies, USA), 24–48 h before analysis. In order to diminish the secretion of endogenously expressed WNTs, cells were pretreated over night with 5 µM of the porcupine inhibitor C59 (2-[4-(2-Methylpyridin-4-yl)phenyl]-N-[4-(pyridin-3-yl)phenyl]acetamide; Abcam) where indicated. Recombinant and purified WNT proteins for stimulation experiments were purchased from BioTechne/R&D Systems.

The full length untagged FZD_4 construct was from www.cdna.org (cat#: #FZD4000000). Human FZD_4 was subcloned into pEGFP-N1, mCherry-N1 or mCerulean-N1 using NheI and BamHI restriction enzymes. Functionality was assessed by recruitment of DVL from cytosolic punctae to the cell membrane upon coexpression (**Supplemental Figure 1**). $G\alpha_s$-GFP and $G\alpha_{i1}$-GFP were provided by Mark Rasenick (University of Chicago, Chicago, IL, USA; (Yu and Rasenick, 2002)); $G\alpha_q$-Venus and $G\alpha_{oA}$-Venus were from Nevin A. Lambert (Georgia Health Sciences University, Augusta, GA, USA (Digby et al., 2006)); $G\alpha_{12/13}$-mCherry were cloned as an N-terminal fusion to the G protein, according to $G\alpha_{13}$-RLucII (Yagi et al., 2011). In detail, $G\alpha_{13}$-mCherry was cloned from pCEFL MYC GFP10 $G\alpha_{13}$ wt (from Silvio

Molecular Pharmacology Fast Forward. Published on July 25, 2016 as DOI: 10.1124/mol.116.104919
This article has not been copyedited and formatted. The final version may differ from this version.

Gutkind) introducing a BglII site with forward primer 5' CCAGATCTGCCACCATGGCGGACTTCCTGCCG 3' and an EcoRI site with reverse primer 5' CCGAATTCTCA CTGTAGCATAAGCTGCTT 3'. The $G\alpha_{13}$ wt was excised by BglII and EcoRI digest and inserted into pmCherry-C1 vector. $G\alpha_{12}$-mCherry was cloned from $G\alpha_{12}$ EE-tagged (internal) (GNA120EI00-02 from www.cdna.org) using 5´ ATGAATTCGACCACCATGTCCGGGGTGGT 3´ and 5´ ATGGATCCTCACTGCAGCATGATGTCCTTCAGGTT 3´ to introduce an EcoRI and BamHI site, respectively. The EE-tagged $G\alpha_{12}$ was excised by EcoRI and BamHI and inserted into pmCherry-C1. Constructs were confirmed by sequencing. Correct membranous localization and activity of the N terminally tagged $G\alpha_{12}$-mCherry and $G\alpha_{13}$-mCherry constructs were verified in HEK293 cells. Membranous localization of the mCherry-tagged constructs indicate correct lipidation of the G proteins (see **Fig.1** and **Supplemental Figure 2,3**). Further, we used a p115-RHOGEF-GFP recruitment assay in the presence and absence of overexpressed $G\alpha_{12}$- and $G\alpha_{13}$-mCherry in combination with lysophosphatidic acid 1 receptor (LPA_1 receptor) to further support functionality of the N terminally tagged G proteins (**Supplemental Figure 2-4**). The pCEFL p115RHOGEF-GFP construct and the extended AU1-tagged RGS domain of p115-RHOGEF (in pCEFL) containing $G\alpha_{12/13}$-selective GAP/RGS activity were from Silvio Gutkind. The LPA_1 receptor-selective antagonist/inverse agonist Ki16425 (3-(4-(4-((1-(2-chlorophenyl)ethoxy)carbonyl)-3-methylisoxazol-5-yl)benzylthio)propanoic acid) (Ohta et al., 2003; Shano et al., 2008) was able to reduce the LPA_1R-induced membrane recruitment of p115-RHOGEF-GFP, supporting its dependence on endogenously produced agonists or constitutive activity of the LPA_1 receptor upon overexpression (**Supplemental Figure 4**). The GFP-KRAS fusion protein of the last 25 aa (RKHKEKMSKDGKKKKKKSKTKCVIM including the farnesylation site) of

Molecular Pharmacology Fast Forward. Published on July 25, 2016 as DOI: 10.1124/mol.116.104919
This article has not been copyedited and formatted. The final version may differ from this version.

KRAS and the fluorescent protein EGFP was provided by Nevin A. Lambert (Lan et al., 2011). DVL1-FLAG was from Madelon M. Maurice (University Medical Center, Utrecht, Netherlands); DVL2-MYC was from S. A. Yanagawa (Kyoto University, Kyoto, Japan); DVL3-FLAG was from Randall T. Moon (University of Washington School of Medicine, Seattle, WA, USA). All constructs were confirmed by sequencing.

For human DVL silencing, pan-DVL siRNA (AAGUCAACAAGAUCACCUUCU) targeting position 1450–1468 of human DVL1, isoform 1; position 1375–1393 of human DVL1, isoform 2; position 1474–1492 of DVL2; and position 1441–1459 of DVL3 or Xeragon (Qiagen, Sweden) control nonsilencing siRNA (AAUUCUCCGAACGUGUCACGU) were added simultaneously with plasmids (Bryja et al., 2008). Cells were transfected at a 3:1:1:1 ratio of receptor:Gα:β:γ plasmids or receptor:DVL plasmids at a ratio of 3:1.

Dual-color Fluorescence Recovery After Photobleaching

The procedure was essentially as described in (Kilander et al., 2014b; Qin et al., 2011; Qin et al., 2008). Cells were grown on 35 mm ECM gel-coated (1:300; Sigma-Aldrich) glass bottom dishes and assessed using a Zeiss 710 laser-scanning microscope. Membranous, tagged FZD_4 was immobilized using avidin-biotin crosslinking. Briefly, cells were incubated 0.5 mg/ml NHS-sulfo-LC-LC-biotin followed by 0.1 mg/ml avidin (ThermoFisher Scientific, Sweden) for 15 min each at room temperature and rinsed 3 times before, between, and after incubations. Washing and incubation steps were performed in crosslinking buffer (CL) buffer (150 mM NaCl, 2.5 mM KCl, 10 mM HEPES, 12 mM glucose, 0.5 mM $CaCl_2$, and 0.5 mM $MgCl_2$, adjusted to pH 8.0). Cellular imaging was performed within 1 h of avidin exposure.

Molecular Pharmacology Fast Forward. Published on July 25, 2016 as DOI: 10.1124/mol.116.104919
This article has not been copyedited and formatted. The final version may differ from this version.

Measurements in which the receptor's mobility was not sufficiently affected by CL were excluded (cutoff: ≥40% FRAP recovery). Images were acquired using a 40x, 1.2 NA C-Apochromat objective and the 488 nm and the 561 nm laser lines were used to excite GFP-Venus and mCherry fluorophores, respectively. For all FZD_4-Gα subunit combinations untagged $\beta\gamma$ subunits were cotransfected. For FRAP experiments, a 2.86x 2.86 µm defined area was placed over the cell plasma membrane and monitored using low-intensity illumination. Care was taken to select for cells that appeared to have more receptor than G protein expressed, taking into account laser power and gain settings and the differences in the fluorescence yield of the fluorescent proteins. After an initial prebleach period, irreversible photobleaching was performed by increasing the laser intensity to 100%. Fluorescent recovery after bleaching was measured using low illumination again, and was measured in total for a time period of 101 s. Average pixel intensity was recorded using the ZEN2013 software, corrected for photobleaching and background fluctuations and normalized to pre-bleached intensity. The mobile fraction (F_m) was calculated with $F_m = (I_P - I_0) / (I_I - I_0)$, where I_I is the initial intensity measured before bleaching, I_0 is the immediate fluorescence intensity after bleaching and I_P is intensity value after recovery of fluorescence. The mobile fraction was determined by averaging fluorescence intensity values obtained between 55-85 seconds.

Förster resonance energy transfer – photoacceptor bleaching

HEK293 cells were seeded on sterile, gelatine-coated coverslips in a 24-well plate, transfected with FZD_4-GFP, untagged $\beta\gamma$ and Gα_{12}- or Gα_{13}-mCherry subunits. The cells were treated with or without WNT-7A (300 ng/ml; 5 min) prior fixation in 4% paraformaldehyde. FRET between FZD_4-GFPand Gα_{12}- or Gα_{13}-mCherry subunits

Molecular Pharmacology Fast Forward. Published on July 25, 2016 as DOI: 10.1124/mol.116.104919
This article has not been copyedited and formatted. The final version may differ from this version.

was performed on an LSM710 (Zeiss), with a 40x water-immersion objective (C-Apochromat, 1.2 NA; Zeiss) by acceptor photobleaching with 100% laser power of a 561-nm diode laser for 20 s. Signal intensity of the photoacceptor (mCherry) was routinely reduced by 80–90%. Images were acquired before and after photobleaching with excitation/emission ranges of 488/493–545 nm (GFP) and 561/562–681 nm (mCherry). Quantification of the GFP emission before and after the photobleaching was determined with region of interest (ROI) analysis in at least 10 individual cells per experiment and condition using the ZEN2013 software. Data were background corrected and adjusted for fluctuations in intensity with an unbleached ROI as reference. FRET efficiency was calculated as $E = [1 - (I_{pre}/I_{post})] \times 100\%$. Control experiments were performed using FZD_4-GFP and myristoylated (MYR)-mCherry to define basal FRET of fluorescent proteins co-expressed in the same cellular compartment.

Dynamic mass redistribution (DMR)

Label-free measurements were performed using the Epic System (Corning) as described previously in detail (Grundmann and Kostenis, 2015; Schroder et al., 2011). In brief, HEK293 cells were seeded onto fibronectin-coated 384 well biosensor plates at a density of 15,000 cells per well in complete growth medium. After 4 hours the medium was exchanged for starvation medium lacking FBS but supplemented with 5µM of the porcupine inhibitor C59 and incubated at 37°C overnight. Cells were washed with HBSS containing 20mM HEPES, 5µM C59 and equilibrated at 37°C for at least 1 hour before compound addition and DMR recording. Experiments were performed 24 – 48 hours after transfection of pcDNA3.1(+) or FZD_4-pEGFP-N1 using FuGENE HD (Promega). HEK293 cells lacking $G\alpha_{12/13}$ were a kind gift of Dr. Asuka

Molecular Pharmacology Fast Forward. Published on July 25, 2016 as DOI: 10.1124/mol.116.104919
This article has not been copyedited and formatted. The final version may differ from this version.

Inoue (Tohoku University, Japan). $G\alpha_{12/13}$, which are encoded by the GNA12 and the GNA13 genes, respectively, were simultaneously targeted by a CRISPR-Cas9 system.

p115-RHOGEF-GFP recruitment assay

HEK293 cells were seeded onto 4-chamber glass bottom dishes (coated with ECM gel 1:300; Sigma-Aldrich) and transfected with combinations of FZD_4-Cerulean, $G\alpha_{12}$- or $G\alpha_{13}$-mCherry, p115-RHOGEF-GFP and untagged $\beta\gamma$ subunits (ratio 3:1:1:1:1). The next day, the living cells were examined by confocal microscopy (Zeiss LSM510; C-Apochromat 40x/1.2W) to visualize the fluorescently tagged proteins using sequential scanning in combination with exitation 405 nm/ emission 420-480 nm, 488 nm/ LP505 nm and 543 nm/ LP 560 nm for Cerulean, GFP and mCherry, respectively. For crosstalk/ bleed through was controlled using cells expressing the single fluorescent proteins. The Zeiss ZEN2013 software was used to generate fluorescence intensity profiles. For quantification of p115-RHOGEF-GFP membrane recruitment, random images were taken at higher magnification. Cell categories “membranous” and “cytosolic” were defined for p115-RHOGEF-GFP distribution and more than 50 (up to several hundred) cells per condition (+/- FZD_4-Cerulean) were counted from three independent experiments. Data are presented as percentage of all counted p115-RHOGEF-GFP-positive cells showing membranous p115-RHOGEF-GFP distribution.

Western Blot Analysis

HEK293T cells were plated in a 24-well plate at a density of 150.000 cells/well, and grown overnight. Cells were transfected using Lipofectamine 2000 or 3000 according

Molecular Pharmacology Fast Forward. Published on July 25, 2016 as DOI: 10.1124/mol.116.104919
This article has not been copyedited and formatted. The final version may differ from this version.

to manufacturer's instructions. For lysis equal amount of a 2x SDS sample buffer were applied to the cells. Protein lysates were analyzed by standard SDS–PAGE/immunoblotting using the following primary antibodies: mouse anti-β-actin (1: 30.000; Sigma-Aldrich #A5441), mouse anti-DVL1 (1:500; Santa Cruz Biotechnology #sc-133525), rabbit anti-DVL2 (1:1000; Cell Signaling Technologies #3216), mouse anti-DVL3 (1:500; Santa Cruz #sc-8027), mouse anti-MYC (1:500, Santa Cruz Biotcehnology #sc-40,), mouse anti-FLAG M2 (1:1000; Sigma-Aldrich #F1804). Signals were detected by HRP-conjugated secondary antibodies (Pierce Biotechnology, USA) and visualized with standard enhanced chemiluminescence detection protocols.

Statistical analysis

Statistical and graphical analyses were performed using Graph Pad Prism 6 software. FRAP data were analyzed by one-way analysis of variance (ANOVA)/post hoc Bonferroni's multiple comparisons or student's t-test. Curve fitting of FRAP data was achieved with a two-phase association non-linear function using the least-square fit. All experiments were repeated at least three times; FRAP data were based on 8-55 regions of interest (ROIs) per data point from at least three independent experiments. The number of ROIs per data point varies because some ROIs are excluded from the analysis for example when visual inspection indicated that cellular movements led to a repositioning of the observed bleached membrane area from the ROI during the recovery phase after photobleaching. The analyzed ROIs originated from individual cells from independent cell transfections. Significance levels are given as: * $p<0.05$; ** $p<0.01$; *** $p<0.001$. Data in FRAP curves and FRAP bar graphs are presented as mean±standard error of the mean (SEM). Quantitative assessment of protein translocation (DVL1-FLAG and p115-RHOGEF-GFP) was done by manual

Molecular Pharmacology Fast Forward. Published on July 25, 2016 as DOI: 10.1124/mol.116.104919
This article has not been copyedited and formatted. The final version may differ from this version.

counting by an observer blinded to the experimental conditions. At least 50 cells in total were counted per experimental condition in three independent experiments. Results are presented in bar graphs as means±SEM. Statistics were done by a one-way analysis of variance (ANOVA) with Tukey test for multiple comparisons.

Molecular Pharmacology Fast Forward. Published on July 25, 2016 as DOI: 10.1124/mol.116.104919
This article has not been copyedited and formatted. The final version may differ from this version.

Results

FZD_4 interacts with the heterotrimeric G proteins $G\alpha_{12}$ and $G\alpha_{13}$ but not $G\alpha_{i1}$, $G\alpha_o$, $G\alpha_s$, $G\alpha_q$

In order to assess the ability of FZD_4 to assemble with heterotrimeric G proteins in an inactive state complex we expressed FZD_4-GFP or FZD_4-mCherry in HEK293T cells. Both constructs showed membrane localization and were able to recruit DVL from a distinct punctuate pattern of cytosolic aggregates to the plasma membrane similar to the full length, untagged human FZD_4 (**Supplemental Figure 1**). Upon co-expression in HEK293T cells, FZD_4 co-localized with fluorescently labelled $G\alpha_{i1}$, $G\alpha_o$, $G\alpha_s$, $G\alpha_q$, $G\alpha_{12}$ and $G\alpha_{13}$ subunits predominantly in the plasma membrane (**Fig. 1**). In order to assess FZD_4–G-protein interaction, we took advantage of a dual-color FRAP (dcFRAP) protocol that enables simultaneous assessment of lateral mobility of two fluorescently tagged proteins (Dorsch et al., 2009; Kilander et al., 2014b; Phair et al., 2004; Qin et al., 2011; Qin et al., 2008) (**Fig. 1**). This experimental setup is based on immobilization of transmembrane proteins by chemical surface crosslinking (CL) with sulfo-NHS-LC-LC-biotin and avidin. In contrast to transmembrane receptors, intracellular proteins, such as the heterotrimeric G proteins, are not directly affected by surface CL in this assay. The mobile fraction of intracellular proteins is reduced only upon interaction with crosslinking-immobilized surface proteins (Kilander et al., 2014b; Qin et al., 2011; Qin et al., 2008). In cells transfected with fluorescently tagged FZD_4, $G\alpha$, and untagged $\beta\gamma$ we found that the mobile fraction of FZD_4 was remarkably reduced by surface crosslinking (**Fig. 1C-H**). In accordance with an inactive state assembly of receptor and G protein, we found that the mobile fraction of $G\alpha_{12}$ and $G\alpha_{13}$ but not that of other representatives of the G protein subfamilies $G\alpha_s$, $G\alpha_{i/o}$, $G\alpha_q$ were affected by surface crosslinking of the receptor (**Fig. 1C-H**). To

Molecular Pharmacology Fast Forward. Published on July 25, 2016 as DOI: 10.1124/mol.116.104919
This article has not been copyedited and formatted. The final version may differ from this version.

verify that these observed effects were selectively dependent on FZD_4 co-expression and to control for general effects of surface CL on G protein mobility, we had previously performed dcFRAP experiments with myristoylated fluorescent proteins as non-receptor control in combination with fluorescently tagged heterotrimeric $G\alpha_i$ proteins (Kilander et al., 2014b). In **Fig. 2**, we show that chemical surface crosslinking in the absence of overexpressed FZD_4 but in the presence of a membrane-anchored fluorescent protein (GFP-KRAS) did not affect lateral mobility of the heterotrimeric $G\alpha_{12}$-mCherry and $G\alpha_{13}$-mCherry proteins in the presence of untagged $\beta\gamma$, indicating that crosslinking of endogenously expressed receptors does not perturb the interpretation of our data. This observation is further supported by the finding that the mobile fraction of $G\alpha_{12}$-mCherry in the presence of FZD_6-GFP is not affected by CL (Kilander et al., 2014b) indicating that even chemical immobilization of an overexpressed transmembrane protein that does not interact with the heterotrimeric G protein leaves the mobile fraction of the G protein unchanged.

The FZD_4-$G\alpha_{12/13}$ complex dissociates upon WNT stimulation

With the purpose to determine whether agonist treatment disrupts the observed FZD_4-$G\alpha_{12/13}$ complex, we stimulated HEK293T cells expressing FZD_4-GFP, untagged $\beta\gamma$ and $G\alpha_{12/13}$-mCherry with commercially available, purified WNTs (300 ng/ml; 0, 5, 10 min; **Fig. 3**). As expected from earlier experiments with FZD_6 and $G\alpha_{i1}$ or $G\alpha_q$ proteins (Kilander et al., 2014b) the previously observed CL-induced reduction of the mobile fraction of the $G\alpha_{12/13}$ proteins was abolished by WNT-3A, -5A, -7A and -10B treatment, indicating dissociation of the inactive state FZD_4-GFP/$G\alpha_{12/13}$-mCherry complex. In order to further support the dcFRAP data on agonist-induced complex dissociation, we employed FRET measurements in fixed HEK293 cells

Molecular Pharmacology Fast Forward. Published on July 25, 2016 as DOI: 10.1124/mol.116.104919
This article has not been copyedited and formatted. The final version may differ from this version.

transfected with FZD_4-GFP, untagged βγ and $G\alpha_{12/13}$-mCherry. Photoacceptor bleaching FRET measurements indicated that energy transfer from FZD_4-GFP to $G\alpha_{12/13}$-mCherry occurred at basal and that FRET decreased with WNT-7A stimulation (300 ng/m; 5 min; **Fig. 4**) indicative of a receptor-G protein dissociation or rearrangement, similar to what was previously observed in the case of FZD_6 and $G\alpha_{i1}$ or $G\alpha_q$ (Kilander et al., 2014b). The negative control coexpressing FZD_4-GFP and myristoylated (MYR)-mCherry defines background levels of basal FRET between fluorescent proteins that are co-expressed in the same cellular compartment but only randomly approaching each other to yield FRET. Importantly, WNT-7A stimulation reduced FRET between FZD_4-GFP and $G\alpha_{12/13}$-mCherry to basal levels resembling those of the negative control. Thus, both the affinity-based dcFRAP assay and the proximity-based FRET assay support FZD_4-G protein interaction and agonist-induced dissociation.

The FZD_4-$G\alpha_{12/13}$ complex is independent of DVL

Since we previously identified DVL as a master regulator of FZD_6-$G\alpha_{i1}$ or FZD_6-$G\alpha_q$ association (Kilander et al., 2014b), we also investigated the role of the scaffold protein DVL for formation of the inactive state assembled complex between FZD_4 and $G\alpha_{12/13}$ by *in vitro* loss- and gain-of-function experiments. On one hand, we overexpressed DVL1, 2, 3 in HEK293T cells expressing FZD_4 and $G\alpha_{12}$-mCherry and untagged βγ-subunits at a plasmid ratio of 3:1:1 receptor:Gαβγ:DVL. On the other hand, we downregulated DVL1, 2, 3 employing panDVL siRNA designed to target all 3 human isoforms of DVL (**Fig. 5**). Thereby, we created cellular systems with low (pan-DVL siRNA), intermediate (endogenous), and high DVL levels (DVL overexpression). When performing dcFRAP experiments in these cellular setups we

Molecular Pharmacology Fast Forward. Published on July 25, 2016 as DOI: 10.1124/mol.116.104919
This article has not been copyedited and formatted. The final version may differ from this version.

found that changed DVL expression levels did not affect FZD_4-$G\alpha_{12}$ complex formation (**Fig. 5**) indicating that the scaffold protein DVL is not required and dispensable for WNT-FZD_4-$G\alpha_{12/13}$ inactive state complex formation.

Analysis of G protein selectivity of FZD_4 and FZD_6 chimeric receptors

Given that prediction of receptor G protein selectivity from the primary GPCR structure is still not possible, we aimed to combine our knowledge from FZD_6 as a receptor selectively interacting with $G\alpha_i$ and $G\alpha_q$ and FZD_4 as a receptor that assembles with $G\alpha_{12/13}$ to shed light on domains required for G protein selectivity in FZDs. Both receptors belong to different homology clusters grouping $FZD_{4,9,10}$ and $FZD_{3,6}$ (Schulte, 2010), and their C termini differ dramatically in length: The FZD_4 C tail comprises 41 aa and the FZD_6 tail consists of 211 aa. The hypothesis for creating FZD_4-FZD_6 tail and FZD_6-FZD_4 tail chimera through a classical domain swap of the C terminal regions, was that exchanging C terminal tails could be accompanied by interchanging G protein-selectivity. In **Fig. 6** dcFRAP data are shown indicating G protein selectivity of the respective chimera. While the G protein-coupling selectivity of the FZD_6-FZD_4 tail chimera was switched from $G\alpha_i$ / $G\alpha_q$ to $G\alpha_{12}$, the FZD_4-FZD_6 tail chimera still preferentially bound to $G\alpha_{12}$ rather than $G\alpha_i$ or $G\alpha_q$.

WNT-induced dynamic mass redistribution in HEK293 depends on $G\alpha_{12/13}$

Recent developments in label-free technologies, such as DMR measurements, allow global analysis of ligand-induced changes in living cells (Grundmann and Kostenis, 2015; Schroder et al., 2011). DMR in living cells presents a holistic view on changes in multiple cellular processes such as protein trafficking, morphological changes, cytosceletal rearrangement, receptor internalization or adhesion (Schroder et al.,

Molecular Pharmacology Fast Forward. Published on July 25, 2016 as DOI: 10.1124/mol.116.104919
This article has not been copyedited and formatted. The final version may differ from this version.

2010), some of which are connected to $G\alpha_{12/13}$ signaling (Worzfeld et al., 2008). To investigate whether DMR technology is competent to visualize the cellular consequences set in motion by WNT-5A upon activation of FZD_4-$G\alpha_{12/13}$ complexes, we utilized HEK293 cells genetically deficient or not in $G\alpha_{12/13}$ and monitored WNT-induced alterations of global cell activity. We observed negative DMR upon stimulation with WNT-5A in vector transfected HEK293 wild-type cells (**Fig. 7A**) indicating interaction of WNT-5A with a molecular target endogenous to the HEK293 cell background. Importantly, overexpression of FZD_4-GFP intensified this response, which substantiates a FZD_4 receptor-dependent WNT-5A mode-of-action (**Fig. 7B**). Strikingly, these responses were completely sensitive to $G\alpha_{12/13}$ protein knock-out (**Fig. 7C,D**) indicative of FZD_4 receptor signaling via $G\alpha_{12/13}$. FZD_4 receptor-independent cell responses induced by the direct adenylate cyclase stimulator forskolin, however, remained unaffected by either $G\alpha_{12/13}$ protein knock-out or FZD_4-GFP overexpression (**Supplemental Figure 5**).

Signaling along a WNT-FZD_4-$G\alpha_{12/13}$-p115RHOGEF signaling axis

In order to link the FZD_4-$G\alpha_{12/13}$ complex functionally to downstream signaling events and to support the idea that FZD_4 indeed mediates the GDP/GTP exchange at $G\alpha_{12/13}$ proteins, we expanded on previous findings identifying p115-RHOGEF as a $G\alpha_{12/13}$ target that physically interacts with the active, GTP-bound α subunit and stimulates its GTPase activity similar to classical regulators of G protein signaling proteins (Hart et al., 1998; Hart et al., 1996; Meyer et al., 2008; Worzfeld et al., 2008). Most importantly, with regard to the functionality of the tagged $G\alpha_{12/13}$-mCherry subunits, correct palmitoylation of $G\alpha_{12/13}$ is required for the G protein's plasma membrane localization and the promotion of p115-RHOGEF recruitment to

Molecular Pharmacology Fast Forward. Published on July 25, 2016 as DOI: 10.1124/mol.116.104919
This article has not been copyedited and formatted. The final version may differ from this version.

the plasma membrane by the active, GTP-bound G protein (Bhattacharyya and Wedegaertner, 2000). Comparable to the results with coexpression of the LPA_1 receptor and $G\alpha_{12/13}$-mCherry (**Supplemental Figure 2-4**) also FZD_4-Cerulean induced p115-RHOGEF-GFP membrane recruitment in combination with $G\alpha_{12/13}$-mCherry (**Fig. 8**). Neither $G\alpha_{12/13}$-mCherry nor FZD_4-Cerulean alone were sufficient to translocate p115-RHOGEF-GFP from a predominantly cytosolic expression pattern to a plasma membrane localization (**Supplemental Figure 2; Fig. 8**). Substantial p115-RHOGEF-GFP membrane localization was only observed when FZD_4-Cerulean was co-expressed with $G\alpha_{12/13}$-mCherry, arguing that receptor-induced activation of $G\alpha_{12/13}$ is required for this process.

In order to dissect the ligand dependence of the response from FZD_4 via $G\alpha_{12/13}$ to p115-RHOGEF-GFP recruitment we disrupted endogenous secretion of WNTs by overnight treatment with the pharmacological porcupine inhibitor C59 (Proffitt et al., 2013). Porcupine was identified as a segment polarity gene giving rise to a multi-span transmembrane protein catalyzing WNT acylation (Kadowaki et al., 1996). Pharmacological inhibition of porcupine is therefore an efficient way to decrease the amount of endogenously produced, functional WNTs to reduce autocrine stimulation (Dodge et al., 2012). This set up is analogous to the reduction of the LPA_1 receptor-induced and $G\alpha_{12/13}$-mediated p115-RHOGEF-GFP recruitment by the LPA_1 receptor-selective antagonist/inverse agonist Ki16425 (**Supplemental Figure 4**). In agreement with that, C59 treatment of FZD_4-Cerulean, $G\alpha_{12/13}$-mCherry and p115-RHOGEF-GFP transfected cells decreased the number of cells showing a membranous localization of p115-RHOGEF-GFP (**Fig. 8**), indicating that the endogenously secreted WNTs signal through FZD_4-GFP and $G\alpha_{12/13}$-mCherry to contribute to p115-RHOGEF-GFP recruitment.

Molecular Pharmacology Fast Forward. Published on July 25, 2016 as DOI: 10.1124/mol.116.104919
This article has not been copyedited and formatted. The final version may differ from this version.

$G\alpha_{12/13}$ need to be activated and GTP-bound to physically interact with p115-RHOGEF and simultaneously p115-RHOGEF exerts GTPase activating protein or RGS activity on the heterotrimeric G protein to mediate inactivation as part of a negative feedback loop (Hart et al., 1998; Kozasa et al., 1998). In order to corroborate the FZD_4-mediated activation of $G\alpha_{12/13}$, we used the p115-RHOGEF-GFP recruitment as readout in cells co-transfected with the extended AU1-tagged regulator of G protein signaling (RGS) domain of p115-RHOGEF, the domain that promotes hydrolysis of GTP to GDP. Compared to cells transfected with FZD_4-GFP, $G\alpha_{12/13}$-mCherry and p115-RHOGEF-GFP, where we observed 23±2% ($G\alpha_{12}$)/ 30±3% ($G\alpha_{13}$) (mean±SEM) cells with membranous p115-RHOGEF-GFP, co-expression of the RGS domain reduced p115-RHOGEF-GFP membrane recruitment to 13±2% ($G\alpha_{12}$)/ 13±3% ($G\alpha_{13}$) corresponding to values in the absence of FZD_4-GFP transfection (14±2% ($G\alpha_{12}$)/ 15±3% ($G\alpha_{13}$)) (**Fig. 9**).

Molecular Pharmacology Fast Forward. Published on July 25, 2016 as DOI: 10.1124/mol.116.104919
This article has not been copyedited and formatted. The final version may differ from this version.

Discussion

In the present study we employed cellular imaging approaches to investigate the interaction of FZD_4 with heterotrimeric G proteins in unprecedented depth. Combining the dcFRAP technique with FRET, we were able to identify FZD_4 as a receptor assembled with $G\alpha_{12}$ and $G\alpha_{13}$ based on experiments in a mammalian cellular system. Cellular imaging experiments were corroborated employing innovative technology enabling DMR measurements in living cells to dissect the role of $G\alpha_{12/13}$ for WNT-induced cellular responses. In addition, we explored the roles of the scaffold protein DVL for FZD_4-G protein assembly and the connection of FZD_4, $G\alpha_{12/13}$ and signaling to RHO via p115-RHOGEF.

Ever since their discovery in *Drosophila melanogaster*, FZDs have been postulated being GPCRs, due to structural and functional resemblance to more conventional Class A, B and C GPCRs (Park et al., 1994; Schulte and Bryja, 2007; Vinson et al., 1989). In support of what was previously surmised, a great amount of functional evidence has been gathered over the past two decades confirming that FZDs can signal as GPCRs (Ahumada et al., 2002; Dijksterhuis et al., 2014; Halleskog et al., 2012; Katanaev and Buestorf, 2009; Katanaev et al., 2005; Kilander et al., 2011; Koval and Katanaev, 2011; Liu et al., 2001; Liu et al., 1999; Schulte, 2010; Sheldahl et al., 2003; Slusarski et al., 1997).

In the case of FZD_4, a receptor that has been attributed a central role in retinal vascularization and related diseases such as familial exudative vitreoretinopathy (FEVR) (Robitaille et al., 2002), no evidence suggesting interaction with heterotrimeric G proteins has been reported so far. Based on our data using a live-cell imaging dcFRAP approach, which has been successfully used to study GPCR-G

Molecular Pharmacology Fast Forward. Published on July 25, 2016 as DOI: 10.1124/mol.116.104919
This article has not been copyedited and formatted. The final version may differ from this version.

protein interactions in the past (Kilander et al., 2014b; Qin et al., 2011; Qin et al., 2008), we show that FZD_4 interacts with $G\alpha_{12/13}$ but not representatives of other G protein subfamilies. The observed selectivity of FZD_4 for one but not all groups of heterotrimeric G proteins underlines the specificity of the dcFRAP assay and supports the use of overexpressed proteins. Since we were able to detect the inactive state assembly of FZD_4 and $G\alpha_{12/13}$ in living cells, we can conclude that this receptor complex is rather stable under the given circumstances. It should be noted, however, that dcFRAP analysis is a population based assay without single molecule sensitivity and that it does not allow definite quantification of the affinity of the receptor to the heterotrimeric G protein. Further, our data do not allow a conclusion about the predominant mode of FZD_4-G protein coupling in cells endogenously expressing the proteins, which could be cell type and receptor expression level dependent. Thus, it remains to be resolved if FZD_4 at endogenous expression levels indeed forms an inactive state complex with $G\alpha_{12/13}$ or if the predominant mode of signaling is based on collision coupling.

In order to understand the structural basis of FZD-G protein selectivity, we performed C terminal tail swap experiments with FZD_4 and FZD_6, of which the latter assembles with $G\alpha_{i/q}$ (Kilander et al., 2014a; Kilander et al., 2014b). While G protein selectivity of FZD_6 with the C terminus of FZD_4 was changed from predominant $G\alpha_i$ or $G\alpha_q$ to $G_{12/13}$, FZD_4 $G\alpha_{12/13}$ selectivity was not affected by exchanging the 41 aa C terminus to the 211 aa C terminus of FZD_6 (**Fig. 6**). Thus it appears that $G\alpha_{12/13}$ assembly can be achieved with structural determinants encoded by the FZD_4 and FZD_6 core irrespective of the C terminal tail. On the other hand, assembly with $G\alpha_i$ or $G\alpha_q$ is neither determined by the FZD_6 C terminus nor the core alone, but it rather requires the combination of both in the intact FZD_6. It should be noted in this context that

Molecular Pharmacology Fast Forward. Published on July 25, 2016 as DOI: 10.1124/mol.116.104919
This article has not been copyedited and formatted. The final version may differ from this version.

some structural features are common to both the FZD_4 and the FZD_6 C terminus, such as the conserved KTxxxW sequence and the potential ability to form a helix 8 (Schulte, 2010).

Furthermore, we found that this novel FZD_4-$G\alpha_{12/13}$ liaison does neither require DVL for the formation of an inactive state assembled complex nor is it sensitive to DVL overexpression. This stands in contrast to previous results, where we defined DVL as an essential component of the FZD_6-$G\alpha_i$/$G\alpha_q$ complex (Kilander et al., 2014b) arguing that the underlying mechanisms of FZDs interacting with heterotrimeric G proteins could be receptor isoform selective.

DMR analysis revealed $G\alpha_{12/13}$-dependent WNT effects in both untransfected and FZD_4-transfected HEK293 cells. It is well known that HEK293 cells endogenously express FZD_4 among other FZDs (Atwood et al., 2011), suggesting that the WNT-$G\alpha_{12/13}$ responses measured in the receptor/G protein overexpression paradigms can occur at endogenous receptor-G protein expression levels. Furthermore, the loss-of-function approach using HEK293 $G\alpha_{12/13}$ knock out cells underlines that the observed FZD_4-$G\alpha_{12/13}$ liaison is not an artifact of receptor/G protein overexpression. On the other hand, these data open the possibility that also other Class FZD receptors expressed in HEK293 cells could mediate signaling via $G\alpha_{12/13}$.

Heterotrimeric $G\alpha_{12/13}$ proteins signal mainly to RHO GTPase-dependent pathways by interacting with several RHOGEFs regulating for example changes in cell shape, migration and adhesion (Worzfeld et al., 2008). In **Fig. 8, 9**, we show that $G\alpha_{12/13}$-induced p115-RHOGEF recruitment to the membrane is induced by FZD_4. Since p115-RHOGEF interacts with the GTP-bound and active form of $G\alpha_{12/13}$ (Hart et al., 1998), which is dissociated from $\beta\gamma$ subunits and the GPCR, this finding strongly

Molecular Pharmacology Fast Forward. Published on July 25, 2016 as DOI: 10.1124/mol.116.104919
This article has not been copyedited and formatted. The final version may differ from this version.

argues that FZD_4 not only passively assembles with $G\alpha_{12/13}$ but that FZD_4 is indeed capable of functionally coupling to $G\alpha_{12/13}$ acting as a GEF on these heterotrimeric G proteins. Given the lack of pharmacological tools for the selective stimulation of or interference with Class Frizzled receptors, we instead used an alternative approach to pinpoint the ligand dependence of the $FZD_4/G\alpha_{12/13}$-mediated p115RHOGEF-GFP recruitment. Pretreatment with porcupine inhibitors dramatically reduces autocrine WNT secretion (Proffitt et al., 2013) and the negative impact of C59 on p115-RHOGEF-GFP membrane localization argues that $FZD_4/G\alpha_{12/13}$ signaling is WNT dependent. In addition, the negative effect of the isolated p115-RHOGEF RGS domain acting as a $G\alpha_{12/13}$-selective GTPase activating protein (Hart et al., 1998; Kozasa et al., 1998) supports the functionality of the WNT-$FZD_4/G\alpha_{12/13}$-p115-RHOGEF signaling axis and its dependence on FZD_4-mediated activation of $G\alpha_{12/13}$.

In summary, our results provide first evidence that FZD_4 and $G\alpha_{12/13}$ functionally interact, that WNTs can dissociate $G\alpha_{12/13}$ from the inactive state complex and that FZD_4-$G\alpha_{12/13}$ mediate RHO signaling through membrane recruitment of p115-RHOGEF. Thus, FZD_4 should be seen as a $G\alpha_{12/13}$–coupled GPCR even though the circumstances that specify WNT signaling through $FZD_4/G\alpha_{12/13}$/p115-RHOGEF signaling axis over the classical WNT/β-catenin pathway need to be defined in more detail.

Molecular Pharmacology Fast Forward. Published on July 25, 2016 as DOI: 10.1124/mol.116.104919
This article has not been copyedited and formatted. The final version may differ from this version.

Acknowledgements

Prof Lars Larsson, Karolinska Institutet, Dept Physiology & Pharmacology (Stockholm, Sweden), is kindly acknowledged for the generous access to the Zeiss LSM510 confocal microscope. We thank Dr Asuka Inoue (Graduate School of Pharmaceutical Sciences, Tohoku University, Sendai City, Japan) for providing parental and $G\alpha_{12/13}$ knock out HEK293 cells. We are grateful to Corning Inc. for their support on the Epic DMR biosensor.

Author contributions

Participated in research design: EA, BH, MG, EK, JSG, GS

Conducted experiments: EA, BH, JP, KS, SJ, MG

Performed data analysis: EA, BH, SJ, JP, KS, GS, MG

Wrote or contributed to the writing of the manuscript: EA, BH, JP, MG, EK, GS

Molecular Pharmacology Fast Forward. Published on July 25, 2016 as DOI: 10.1124/mol.116.104919
This article has not been copyedited and formatted. The final version may differ from this version.

References

Ahumada A, Slusarski DC, Liu X, Moon RT, Malbon CC and Wang HY (2002) Signaling of rat Frizzled-2 through phosphodiesterase and cyclic GMP. *Science* **298**(5600): 2006-2010.

Angers S and Moon RT (2009) Proximal events in Wnt signal transduction. *Nat Rev Mol Cell Biol* **10**(7): 468-477.

Atwood BK, Lopez J, Wager-Miller J, Mackie K and Straiker A (2011) Expression of G protein-coupled receptors and related proteins in HEK293, AtT20, BV2, and N18 cell lines as revealed by microarray analysis. *BMC genomics* **12**: 14.

Ayoub MA, Al-Senaidy A and Pin JP (2012) Receptor-G protein interaction studied by bioluminescence resonance energy transfer: lessons from protease-activated receptor 1. *Frontiers in endocrinology* **3**: 82.

Aznar N, Midde KK, Dunkel Y, Lopez-Sanchez I, Pavlova Y, Marivin A, Barbazan J, Murray F, Nitsche U, Janssen KP, Willert K, Goel A, Abal M, Garcia-Marcos M and Ghosh P (2015) Daple is a novel non-receptor GEF required for trimeric G protein activation in Wnt signaling. *eLife* **4**: e07091.

Bhattacharyya R and Wedegaertner PB (2000) Galpha 13 requires palmitoylation for plasma membrane localization, Rho-dependent signaling, and promotion of p115-RhoGEF membrane binding. *J Biol Chem* **275**(20): 14992-14999.

Bryja V, Schambony A, Cajanek L, Dominguez I, Arenas E and Schulte G (2008) Beta-arrestin and casein kinase 1/2 define distinct branches of non-canonical WNT signalling pathways. *EMBO Rep* **9**(12): 1244-1250.

Clevers H and Nusse R (2012) Wnt/beta-catenin signaling and disease. *Cell* **149**(6): 1192-1205.

Digby GJ, Lober RM, Sethi PR and Lambert NA (2006) Some G protein heterotrimers physically dissociate in living cells. *Proc Natl Acad Sci U S A* **103**(47): 17789-17794.

Dijksterhuis JP, Baljinnyam B, Stanger K, Sercan HO, Ji Y, Andres O, Rubin JS, Hannoush RN and Schulte G (2015) Systematic Mapping of WNT-Frizzled Interactions Reveals Functional Selectivity by Distinct WNT-Frizzled Pairs. *J Biol Chem*.

Dijksterhuis JP, Petersen J and Schulte G (2014) WNT/Frizzled signalling: receptor-ligand selectivity with focus on FZD-G protein signalling and its physiological relevance: IUPHAR Review 3. *British journal of pharmacology* **171**(5): 1195-1209.

Dodge ME, Moon J, Tuladhar R, Lu J, Jacob LS, Zhang LS, Shi H, Wang X, Moro E, Mongera A, Argenton F, Karner CM, Carroll TJ, Chen C, Amatruda JF and Lum L (2012) Diverse chemical scaffolds support direct inhibition of the membrane-bound O-acyltransferase porcupine. *J Biol Chem* **287**(27): 23246-23254.

Dorsch S, Klotz KN, Engelhardt S, Lohse MJ and Bunemann M (2009) Analysis of receptor oligomerization by FRAP microscopy. *Nat Methods* **6**(3): 225-230.

Gales C, Rebois RV, Hogue M, Trieu P, Breit A, Hebert TE and Bouvier M (2005) Real-time monitoring of receptor and G-protein interactions in living cells. *Nat Methods* **2**(3): 177-184.

Gales C, Van Durm JJ, Schaak S, Pontier S, Percherancier Y, Audet M, Paris H and Bouvier M (2006) Probing the activation-promoted structural rearrangements in preassembled receptor-G protein complexes. *Nat Struct Mol Biol* **13**(9): 778-786.

Grundmann M and Kostenis E (2015) Label-free biosensor assays in GPCR screening. *Methods Mol Biol* **1272**: 199-213.

Halleskog C, Dijksterhuis JP, Kilander MB, Becerril-Ortega J, Villaescusa JC, Lindgren E, Arenas E and Schulte G (2012) Heterotrimeric G protein-dependent WNT-5A signaling to ERK1/2 mediates distinct aspects of microglia proinflammatory transformation. *J Neuroinflammation* **9**(1): 111.

Hart MJ, Jiang X, Kozasa T, Roscoe W, Singer WD, Gilman AG, Sternweis PC and Bollag G (1998) Direct stimulation of the guanine nucleotide exchange activity of p115 RhoGEF by Galpha13. *Science* **280**(5372): 2112-2114.

Hart MJ, Sharma S, elMasry N, Qiu RG, McCabe P, Polakis P and Bollag G (1996) Identification of a novel guanine nucleotide exchange factor for the Rho GTPase. *J Biol Chem* **271**(41): 25452-25458.

He X, Semenov M, Tamai K and Zeng X (2004) LDL receptor-related proteins 5 and 6 in Wnt/beta-catenin signaling: arrows point the way. *Development* **131**(8): 1663-1677.

Hein P, Frank M, Hoffmann C, Lohse MJ and Bunemann M (2005) Dynamics of receptor/G protein coupling in living cells. *EMBO J* **24**(23): 4106-4114.

Kadowaki T, Wilder E, Klingensmith J, Zachary K and Perrimon N (1996) The segment polarity gene porcupine encodes a putative multitransmembrane protein involved in Wingless processing. *Genes Dev* **10**(24): 3116-3128.

Katanaev VL and Buestorf S (2009) Frizzled Proteins are bona fide G Protein-Coupled Receptors. *Nature Precedings* **hdl:10101/npre.2009.2765.1**.

Katanaev VL, Ponzielli R, Semeriva M and Tomlinson A (2005) Trimeric G protein-dependent frizzled signaling in Drosophila. *Cell* **120**(1): 111-122.

Kilander MB, Dahlstrom J and Schulte G (2014a) Assessment of Frizzled 6 membrane mobility by FRAP supports G protein coupling and reveals WNT-Frizzled selectivity. *Cell Signal* **26**(9): 1943-1949.

Kilander MB, Petersen J, Andressen KW, Ganji RS, Levy FO, Schuster J, Dahl N, Bryja V and Schulte G (2014b) Disheveled regulates precoupling of heterotrimeric G proteins to Frizzled 6. *FASEB J*.

Kilander MBC, Dijksterhuis JP, Ganji RS, Bryja V and Schulte G (2011) WNT-5A stimulates the GDP/GTP exchange at pertussis toxin-sensitive heterotrimeric G proteins. *Cellular Signalling* **23**(3): 550-554.

Koval A and Katanaev VL (2011) Wnt3a stimulation elicits G-protein-coupled receptor properties of mammalian Frizzled proteins. *Biochem J* **433**(3): 435-440.

Kozasa T, Jiang X, Hart MJ, Sternweis PM, Singer WD, Gilman AG, Bollag G and Sternweis PC (1998) p115 RhoGEF, a GTPase activating protein for Galpha12 and Galpha13. *Science* **280**(5372): 2109-2111.

Lan TH, Kuravi S and Lambert NA (2011) Internalization dissociates beta2-adrenergic receptors. *PLoS One* **6**(2): e17361.

Liu T, DeCostanzo AJ, Liu X, Wang H, Hallagan S, Moon RT and Malbon CC (2001) G protein signaling from activated rat frizzled-1 to the beta-catenin-Lef-Tcf pathway. *Science* **292**(5522): 1718-1722.

Liu X, Liu T, Slusarski DC, Yang-Snyder J, Malbon CC, Moon RT and Wang H (1999) Activation of a frizzled-2/beta-adrenergic receptor chimera promotes Wnt signaling and differentiation of mouse F9 teratocarcinoma cells via Galphao and Galphat. *Proc Natl Acad Sci U S A* **96**(25): 14383-14388.

Macdonald BT, Semenov MV and He X (2007) SnapShot: Wnt/beta-catenin signaling. *Cell* **131**(6): 1204.

Meyer BH, Freuler F, Guerini D and Siehler S (2008) Reversible translocation of p115-RhoGEF by G(12/13)-coupled receptors. *J Cell Biochem* **104**(5): 1660-1670.

Neubig RR (1994) Membrane organization in G-protein mechanisms. *FASEB J* **8**(12): 939-946.

Nobles M, Benians A and Tinker A (2005) Heterotrimeric G proteins precouple with G protein-coupled receptors in living cells. *Proc Natl Acad Sci U S A* **102**(51): 18706-18711.

Nusse R (2003) Wnts and Hedgehogs: lipid-modified proteins and similarities in signaling mechanisms at the cell surface. *Development* **130**(22): 5297-5305.

Offermanns S, Mancino V, Revel JP and Simon MI (1997) Vascular system defects and impaired cell chemokinesis as a result of Galpha13 deficiency. *Science* **275**(5299): 533-536.

Ohta H, Sato K, Murata N, Damirin A, Malchinkhuu E, Kon J, Kimura T, Tobo M, Yamazaki Y, Watanabe T, Yagi M, Sato M, Suzuki R, Murooka H, Sakai T, Nishitoba T, Im DS, Nochi H, Tamoto K, Tomura H and Okajima F (2003) Ki16425, a subtype-selective antagonist for EDG-family lysophosphatidic acid receptors. *Mol Pharmacol* **64**(4): 994-1005.

Oldham WM and Hamm HE (2008) Heterotrimeric G protein activation by G-protein-coupled receptors. *Nat Rev Mol Cell Biol* **9**(1): 60-71.

Park WJ, Liu J and Adler PN (1994) The frizzled gene of Drosophila encodes a membrane protein with an odd number of transmembrane domains. *Mech Dev* **45**(2): 127-137.

Phair RD, Gorski SA and Misteli T (2004) Measurement of dynamic protein binding to chromatin in vivo, using photobleaching microscopy. *Chromatin and Chromatin Remodeling Enzymes, Pt A* **375**: 393-414.

Proffitt KD, Madan B, Ke Z, Pendharkar V, Ding L, Lee MA, Hannoush RN and Virshup DM (2013) Pharmacological inhibition of the Wnt acyltransferase PORCN prevents growth of WNT-driven mammary cancer. *Cancer Res* **73**(2): 502-507.

Qin K, Dong C, Wu G and Lambert NA (2011) Inactive-state preassembly of G(q)-coupled receptors and G(q) heterotrimers. *Nat Chem Biol* **7**(10): 740-747.

Qin K, Sethi PR and Lambert NA (2008) Abundance and stability of complexes containing inactive G protein-coupled receptors and G proteins. *FASEB J* **22**(8): 2920-2927.

Rasmussen SG, DeVree BT, Zou Y, Kruse AC, Chung KY, Kobilka TS, Thian FS, Chae PS, Pardon E, Calinski D, Mathiesen JM, Shah ST, Lyons JA, Caffrey M, Gellman SH, Steyaert J, Skiniotis G, Weis WI, Sunahara RK and Kobilka BK (2011) Crystal structure of the b2 adrenergic receptor-Gs protein complex. *Nature* **477**(7366): 549-555.

Robitaille J, MacDonald ML, Kaykas A, Sheldahl LC, Zeisler J, Dube MP, Zhang LH, Singaraja RR, Guernsey DL, Zheng B, Siebert LF, Hoskin-Mott A, Trese MT, Pimstone SN, Shastry BS, Moon RT, Hayden MR, Goldberg YP and Samuels ME (2002) Mutant frizzled-4 disrupts retinal angiogenesis in familial exudative vitreoretinopathy. *Nat Genet* **32**(2): 326-330.

Schroder R, Janssen N, Schmidt J, Kebig A, Merten N, Hennen S, Muller A, Blattermann S, Mohr-Andra M, Zahn S, Wenzel J, Smith NJ, Gomeza J, Drewke C, Milligan G, Mohr K and Kostenis E (2010) Deconvolution of complex G protein-coupled receptor signaling in live cells using dynamic mass redistribution measurements. *Nature biotechnology* **28**(9): 943-949.

Schroder R, Schmidt J, Blattermann S, Peters L, Janssen N, Grundmann M, Seemann W, Kaufel D, Merten N, Drewke C, Gomeza J, Milligan G, Mohr K and Kostenis E (2011) Applying label-free dynamic mass redistribution technology to frame signaling of G protein-coupled receptors noninvasively in living cells. *Nat Protoc* **6**(11): 1748-1760.

Schulte G (2010) International Union of Basic and Clinical Pharmacology. LXXX. The class Frizzled receptors. *Pharmacol Rev* **62**(4): 632-667.

Schulte G (2015) Frizzleds and WNT/beta-catenin signaling - The black box of ligand-receptor selectivity, complex stoichiometry and activation kinetics. *Eur J Pharmacol*.

Schulte G and Bryja V (2007) The Frizzled family of unconventional G-protein-coupled receptors. *Trends Pharmacol Sci* **28**(10): 518-525.

Semenov MV, Habas R, Macdonald BT and He X (2007) SnapShot: Noncanonical Wnt Signaling Pathways. *Cell* **131**(7): 1378.

Shano S, Hatanaka K, Ninose S, Moriyama R, Tsujiuchi T and Fukushima N (2008) A lysophosphatidic acid receptor lacking the PDZ-binding domain is constitutively active and stimulates cell proliferation. *Biochim Biophys Acta* **1783**(5): 748-759.

Shastry BS (2010) Genetic susceptibility to advanced retinopathy of prematurity (ROP). *Journal of biomedical science* **17**: 69.

Sheldahl LC, Park M, Malbon CC and Moon RT (1999) Protein kinase C is differentially stimulated by Wnt and Frizzled homologs in a G-protein-dependent manner. *Current biology : CB* **9**(13): 695-698.

Sheldahl LC, Slusarski DC, Pandur P, Miller JR, Kuhl M and Moon RT (2003) Dishevelled activates Ca2+ flux, PKC, and CamKII in vertebrate embryos. *J Cell Biol* **161**(4): 769-777.

Sivaraj KK, Takefuji M, Schmidt I, Adams RH, Offermanns S and Wettschureck N (2013) G13 controls angiogenesis through regulation of VEGFR-2 expression. *Dev Cell* **25**(4): 427-434.

Slusarski DC, Corces VG and Moon RT (1997) Interaction of Wnt and a Frizzled homologue triggers G-protein-linked phosphatidylinositol signalling. *Nature* **390**(6658): 410-413.

Tamai K, Semenov M, Kato Y, Spokony R, Liu C, Katsuyama Y, Hess F, Saint-Jeannet JP and He X (2000) LDL-receptor-related proteins in Wnt signal transduction. *Nature* **407**(6803): 530-535.

Toomes C, Downey LM, Bottomley HM, Mintz-Hittner HA and Inglehearn CF (2005) Further evidence of genetic heterogeneity in familial exudative vitreoretinopathy; exclusion of EVR1, EVR3, and EVR4 in a large autosomal dominant pedigree. *The British journal of ophthalmology* **89**(2): 194-197.

van Amerongen R and Nusse R (2009) Towards an integrated view of Wnt signaling in development. *Development* **136**(19): 3205-3214.

Warden SM, Andreoli CM and Mukai S (2007) The Wnt signaling pathway in familial exudative vitreoretinopathy and Norrie disease. *Seminars in ophthalmology* **22**(4): 211-217.

Wehrli M, Dougan ST, Caldwell K, O'Keefe L, Schwartz S, Vaizel-Ohayon D, Schejter E, Tomlinson A and DiNardo S (2000) arrow encodes an LDL-receptor-related protein essential for Wingless signalling. *Nature* **407**(6803): 527-530.

Vinson CR, Conover S and Adler PN (1989) A Drosophila tissue polarity locus encodes a protein containing seven potential transmembrane domains. *Nature* **338**(6212): 263-264.

Worzfeld T, Wettschureck N and Offermanns S (2008) G(12)/G(13)-mediated signalling in mammalian physiology and disease. *Trends Pharmacol Sci* **29**(11): 582-589.

Xu Q, Wang Y, Dabdoub A, Smallwood PM, Williams J, Woods C, Kelley MW, Jiang L, Tasman W, Zhang K and Nathans J (2004) Vascular development in the retina and inner ear: control by Norrin and Frizzled-4, a high-affinity ligand-receptor pair. *Cell* **116**(6): 883-895.

Yagi H, Tan W, Dillenburg-Pilla P, Armando S, Amornphimoltham P, Simaan M, Weigert R, Molinolo AA, Bouvier M and Gutkind JS (2011) A synthetic biology approach reveals a CXCR4-G13-Rho signaling axis driving transendothelial migration of metastatic breast cancer cells. *Sci Signal* **4**(191): ra60.

Ye X, Wang Y, Cahill H, Yu M, Badea TC, Smallwood PM, Peachey NS and Nathans J (2009) Norrin, frizzled-4, and Lrp5 signaling in endothelial cells controls a genetic program for retinal vascularization. *Cell* **139**(2): 285-298.

Yu JZ and Rasenick MM (2002) Real-time visualization of a fluorescent G(alpha)(s): dissociation of the activated G protein from plasma membrane. *Mol Pharmacol* **61**(2): 352-359.

Molecular Pharmacology Fast Forward. Published on July 25, 2016 as DOI: 10.1124/mol.116.104919
This article has not been copyedited and formatted. The final version may differ from this version.

Footnotes

- Financial support: The study was financially supported by grants from Karolinska Institutet, Karolinska Institutet's Eye Disease Research Foundation, the Board of Doctoral Education at Karolinska Institutet (JP, BH), the Swedish Research Council [2011-2435, 2013-5708, 2015-02899], the Swedish Cancer Society [project grants CAN 2011/690, CAN 2014/659], the Knut & Alice Wallenberg Foundation [KAW2008.0149] and the KI-NIH Joint PhD program in Neuroscience (EA), the Czech Science Foundation [13-32990S], the Program "KI-MU" [CZ.1.07/2.3.00/20.0180] co-financed from European Social Fund and the state budget of the Czech Republic and the Marie Curie ITN WntsApp [608180]; www.wntsapp.eu. This research was supported in part by the Intramural Research Program [Z01DE00551] of the National Institutes of Health, National Institute of Dental and Craniofacial Research (NIDCR). SJ was supported by the ERASMUS+ program.
- For reprint requests contact Gunnar Schulte, Karolinska Institutet, Dept. Physiology & Pharmacology, Sec. Receptor Biology & Signaling, Nanna Svartz väg 2, S-171 77 Stockholm, Sweden. e-mail: gunnar.schulte@ki.se
- Elisa Arthofer and Belma Hot contributed equally

Molecular Pharmacology Fast Forward. Published on July 25, 2016 as DOI: 10.1124/mol.116.104919
This article has not been copyedited and formatted. The final version may differ from this version.

Figure Legends:

Fig. 1: Dual-color FRAP (dcFRAP) in combination with chemical cell surface crosslinking reveals FZD_4-$G\alpha_{12/13}$ complex formation. (**A**) HEK293T cells express fluorescently tagged FZD4 predominantly in the cell membrane. Size bar = 10 µm. (**B**) Double color FRAP (dcFRAP) experiments are done in cells co-transfected with fluorescently tagged FZD_4, $G\alpha$ subunits and untagged $\beta\gamma$ subunits. Micrographs show FZD_4-GFP and $G\alpha_{12}$-mCherry before, shortly after and about 100 s after the high laser power photobleaching in a region of interest (white lines). Surface proteins are chemically crosslinked (CL) by Sulfo-NHS-LC-LC-biotin and avidin. Size bar = 2 µm. (**C-H**) The figure includes a schematic presentation clarifying the experimental setup, a confocal micrograph showing HEK293T cells co-expressing FZD_4 with the respective $G\alpha$ subunit (size bar = 10 µm), fluorescence intensity curves before (grey) and after (red) CL for both FZD_4 and the respective G protein and a bar graph summarizing the mobile fractions of FZD_4 and the $G\alpha$ subunit under each experimental condition. Color code for mobile fractions (consistent throughout the manuscript): white – FZD_4 before CL; red hatched – FZD_4 after CL; grey – $G\alpha$ before CL; grey + red hatched – $G\alpha$ after CL. *** $p<0.001$ (n=3). Error bars provide standard error of the mean (SEM); ns – not significant.

Fig. 2: Non-receptor control ensures that the mobile fraction of $G\alpha_{12/13}$-mCherry is not affected by chemical surface crosslinking in the absence of FZD_4.
HEK293 cells expressing farnesylated GFP-KRAS, untagged $\beta\gamma$ subunits and N-terminally tagged $G\alpha_{12}$-mCherry were used for a dcFRAP assay using chemical surface crosslinking (CL) with Sulfo-NHS-LC-LC-biotin and avidin as described in Fig.

Molecular Pharmacology Fast Forward. Published on July 25, 2016 as DOI: 10.1124/mol.116.104919
This article has not been copyedited and formatted. The final version may differ from this version.

1. CL did neither affect the mobile fraction of GFP-KRAS nor that of $G\alpha_{12}$-mCherry (A) or $G\alpha_{13}$-mCherry (B). The figure includes a schematic presentation clarifying the experimental set up, a confocal micrograph showing HEK293T cells co-expressing GFP-KRAS with the $G\alpha_{12}$-mCherry (A) or $G\alpha_{13}$-mCherry (B; size bars = 10 µm), fluorescence intensity curves before (grey) and after (red) CL for both GFP-KRAS and $G\alpha_{12/13}$-mCherry and a bar graph summarizing the mobile fractions of GFP-KRAS and the $G\alpha$ subunit under each experimental condition. The data verify that the decrease in G protein mobile fraction observed for $G\alpha_{12/13}$-mCherry in the presence of FZD_4-GFP is not evoked by CL of endogenously expressed receptors. Error bars provide standard error of the mean (SEM); ns – not significant. *** $p<0.001$. Bar graph summarizes measurements from at least four independent experiments each including data from several individual cells.

Fig. 3: FZD_4-$G\alpha_{12/13}$ complex dissociates upon WNT stimulation. dcFRAP experiments were performed in HEK293T cells expressing FZD_4-GFP and $G\alpha_{12}$ or $G\alpha_{13}$-mCherry. The mobile fractions of the two proteins were determined before crosslinking and after (CL) as well as after 5 and 10 min after CL/WNT stimulation (all WNTs at 300 ng/ml). Kinetic analysis of the mobile fraction indicates dissociation of the receptor G protein complex upon WNT stimulation. For WNT-5A (Fig. A, B), we have investigated WNT-induced dissociation from FZD_4-GFP for $G\alpha_{12}$ or $G\alpha_{13}$-mCherry. For the other WNTs (WNT-3A, -7A, 10B), only WNT-induced $G\alpha_{12}$-mCherry dissociation was measured (Fig. C-E). * $p<0.05$, ** $p<0.01$, *** $p<0.001$ (n=3). Error bars provide SEM; ns – not significant. Bar graph summarizes measurements from at least three independent experiments each including data from several individual cells.

Molecular Pharmacology Fast Forward. Published on July 25, 2016 as DOI: 10.1124/mol.116.104919
This article has not been copyedited and formatted. The final version may differ from this version.

Fig. 4: Förster resonance energy transfer (FRET) analysis supports WNT-evoked FZD_4-$G\alpha_{12/13}$ complex dissociation. (A) FRET analysis performed in HEK293 cells expressing FZD_4-GFP, untagged $\beta\gamma$ subunits and either $G\alpha_{12}$- or $G\alpha_{13}$-mCherry indicates that FRET between GFP and mCherry decreased in response to WNT-7A stimulation (300 ng/ml; 5 min). FRET measurements were performed with photoacceptor bleaching in fixed cells. Open bars show FRET between GFP and mCherry in the absence of WNT stimulation. Filled bars show FRET upon WNT stimulation. The bar graph summarizes data from three independent experiments with a minimum of 27 ROIs from different cells analyzed per individual experiment and condition. Bars and error bars provide the mean±SEM, respectively. * $p<0.05$; ** $p<0.001$. (B) illustrates the experimental setup schematically.

Fig. 5: DVL does not play a central role for FZD_4-$G\alpha_{12/13}$ complex formation (**A, B**) DVL1-FLAG, DVL2-MYC, DVL3-FLAG were co-expressed in HEK293T cells. Cells that were used for dcFRAP were lysed afterwards to assess DVL1, 2, 3 levels in cellular lysates by immunoblotting using anti-FLAG or anti-MYC antibodies. α-tubulin was used as loading control. (**B**) shows dcFRAP experiments in cells co-expressing FZD_4-GFP and $G\alpha_{12}$-mCherry in the presence of DVL1, 2, or 3. Downregulation of DVL1, 2, 3 by using pan-DVL siRNA did not affect FZD_4-$G\alpha_{12/13}$ assembly. Bar graphs summarize dcFRAP measurements from three independent experiments each including data from several individual cells. Densitometry analysis of three independent experiments employing panDVL siRNA and control indicated that DVL1, 2, 3, were routinely reduced by 35-56 % (values in % reduction in DVL1, 2, 3 band intensity by panDVL siRNA compared to ctrl siRNA (mean±SEM): DVL1 (40±8%); DVL2 (56±2%); DVL3 (35±4%)). For a graphical presentation of the DVL1,

Molecular Pharmacology Fast Forward. Published on July 25, 2016 as DOI: 10.1124/mol.116.104919
This article has not been copyedited and formatted. The final version may differ from this version.

2, 3 levels in ctrl and panDVL siRNA treated cells (N=3) see **Supplemental Figure 6**. (**C**) Immunoblotting indicates reduced expression of the 3 endogenous DVL isoforms in HEK293T cells used for dcFRAP. (**D**) dcFRAP analysis in cells co-expressing FZD_4-GFP and $G\alpha_{12}$-mCherry shows no change in the mobile fraction of $G\alpha_{12}$-mCherry upon CL in cells with reduced levels of DVL. *** $p<0.001$ (n=3). Error bars provide SEM; ns – not significant. Bar graphs summarize measurements from three independent experiments each including data from several individual cells.

Fig. 6: C terminal domain swapping between FZD_4 and FZD_6. (**A**) Schematic presentation of the exchange strategy of the C termini between FZD_4 and FZD_6, resulting in $FZD_{4\text{-}6}$ C terminal tail and $FZD_{6\text{-}4}$ C terminal tail. (**B**) shows the primary structure of human FZD_4 and FZD_6. Green –highlights the conserved KTxxxW sequence involved in DVL binding on the presumptive helix 8. Bold marks the terminal PDZ ligand domain. dcFRAP experiments in HEK293T cells co-expressing $FZD_{4\text{-}6}$-GFP and $G\alpha_{12}$-mCherry, $FZD_{4\text{-}6}$-mCherry and $G\alpha_{i1}$-GFP or $FZD_{4\text{-}6}$-mCherry and $G\alpha_q$-Venus (**B**) and $FZD_{6\text{-}4}$-GFP and $G\alpha_{12}$-mCherry, $FZD_{6\text{-}4}$-mCherry and $G\alpha_{i1}$-GFP or $FZD_{6\text{-}4}$-mCherry and $G\alpha_q$-Venus reveals predominant assembly with $G\alpha_{12}$ of the chimeric receptors. *** $p<0.001$ (n=3). Bar graphs show mean±SEM.

Fig. 7: WNT-induced dynamic mass redistribution depends on $G\alpha_{12/13}$ and FZD4-GFP. HEK293 wild-type cells and HEK293 cells lacking $G\alpha_{12/13}$ were stimulated with increasing amounts of WNT-5A (100, 300, 1000 ng/ml). Changes in DMR were recorded over time. The apparent negative, WNT-5A-induced DMR responses in empty vector (**A**) or FZD_4-GFP transfected (**B**) HEK293 cells were not observed in the absence of $G\alpha_{12/13}$ proteins (**C, D**). Experiments were done after

Molecular Pharmacology Fast Forward. Published on July 25, 2016 as DOI: 10.1124/mol.116.104919
This article has not been copyedited and formatted. The final version may differ from this version.

overnight treatment with the porcupine inhibitor C59 (5 µM) at 37°C. Shown are representative traces (N=3), buffer corrected and measured in triplicates + SEM. See **Supplemental Figure 5** for expression levels of FZD_4-GFP and forskolin-induced DMR responses of wt and $G\alpha_{12/13}$-knock out HEK293 cells.

Fig. 8: FZD_4 induces p115-RHOGEF-GFP membrane recruitment in a $G\alpha_{12/13}$-and WNT-dependent manner. (**A, B, F, I**) HEK293 cells were cotransfected with combinations of FZD_4-Cerulean, $G\alpha_{12}$ or $G\alpha_{13}$-mCherry and p115-RHOGEF-GFP and examined by live-cell confocal imaging. p115-RHOGEF-GFP showed an even cytosolic distribution when expressed alone or in combination with either $G\alpha_{12}$/$G\alpha_{13}$-mCherry or FZD_4-Cerulean (see **Supplemental Figure 2**). The combination of FZD_4-Cerulean and either $G\alpha_{12}$ or $G\alpha_{13}$-mCherry increased p115-RHOGEF-GFP plasma membrane localization. Quantification of the FZD_4-Cerulean-dependent p115-RHOGEF-GFP recruitment was done by counting cells showing membranous vs cytosolic p115-RHOGEF-GFP distribution. Data from three independent experiments (>300 cells from several visual fields counted per condition for each individual experiment) are presented in the bar graphs (**C, G**). Data represent cells with a membranous p115-RHOGEF-GFP localization calculated as percentage of total p115-RHOGEF-GFP-positive cells counted. In combination with the porcupine inhibitor C59 (5 µM; overnight treatment), FZD_4-Cerulean-induced and $G\alpha_{12}$- or $G\alpha_{13}$-mCherry-mediated p115-RHOGEF-GFP recruitment was significantly reduced. Error bars provide SEM. *** $p<0.001$ (N=3).Cellular distribution profiles of p115-RHOGEF-GFP (green) and $G\alpha_{12}$ or $G\alpha_{13}$-mCherry (red) fluorescence intensity along a line drawn over a single cell shown in (**A, B, F, I** – see arrow) in either the absence or

Molecular Pharmacology Fast Forward. Published on July 25, 2016 as DOI: 10.1124/mol.116.104919
This article has not been copyedited and formatted. The final version may differ from this version.

presence FZD_4-Cerulean are shown in (**D, E, H, J**). Size bars, 10 µm.

Fig. 9: FZD_4-induced and $G\alpha_{12/13}$-mediated p115-RHOGEF-GFP membrane recruitment depends on activation of the heterotrimeric $G\alpha_{12/13}$ proteins.

HEK293 cells were transfected with FZD_4-Cerulean, $G\alpha_{12}$- (**A**) or $G\alpha_{13}$-mCherry (**B**) and p115-RHOGEF-GFP either without or with the isolated AU1-tagged RGS domain of p115-RHOGEF-RGS. Cells presenting membranous p115-RHOGEF-GFP localization were counted and data from four independent experiments were summarized in the bar graph. More than 50 cells were counted for each condition in each independent experiment. Values give mean±SEM. (**C**) Cells used for quantification of p115-RHOGEF-GFP recruitment were lysed and immunoblotted for vinculin (loading control) and anti-AU1 to detect the tagged-RGS domain of p115-RHOGEF.

Molecular Pharmacology Fast Forward. Published on July 25, 2016 as DOI: 10.1124/mol.116.104919
This article has not been copyedited and formatted. The final version may differ from this version.

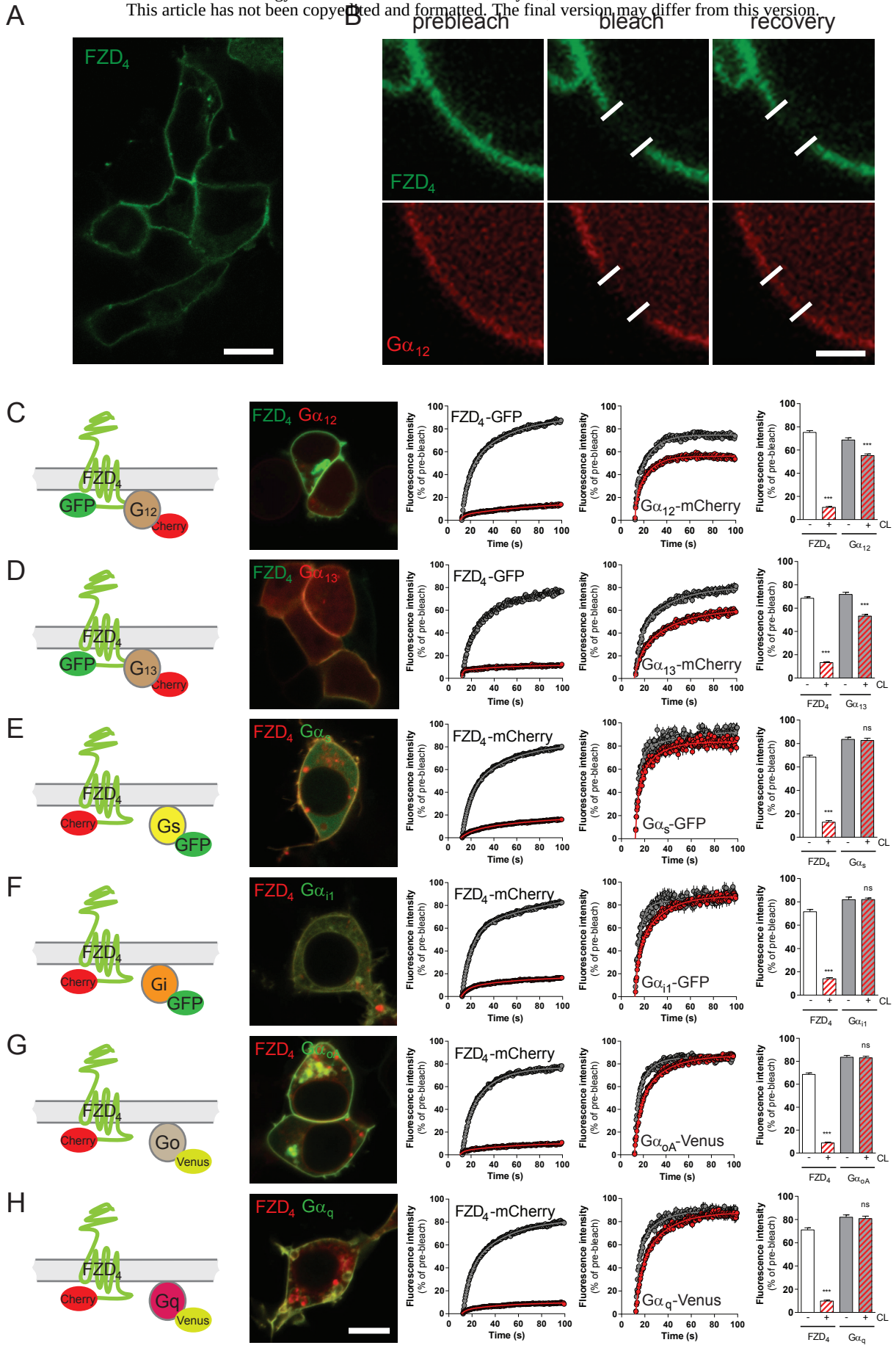

Fig. 1

Molecular Pharmacology Fast Forward. Published on July 25, 2016 as DOI: 10.1124/mol.116.104919
This article has not been copyedited and formatted. The final version may differ from this version.

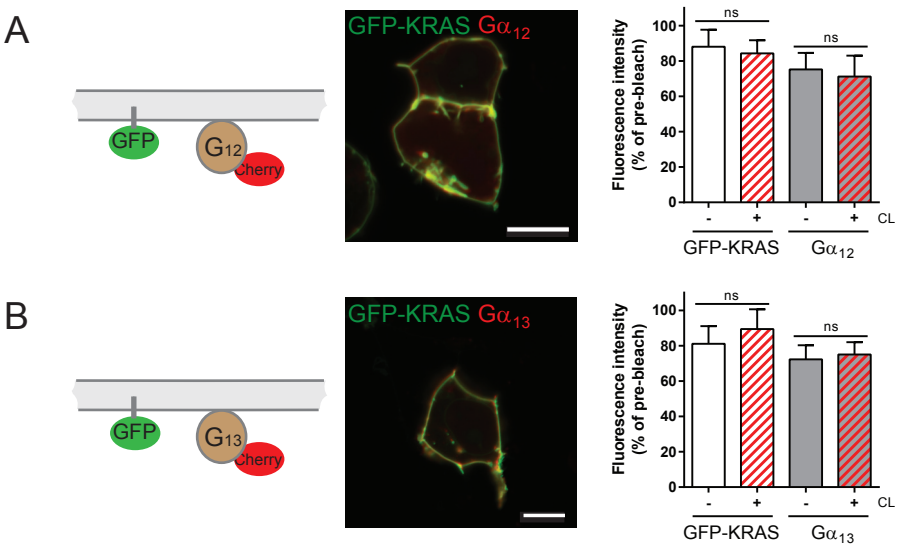

Fig. 2

Molecular Pharmacology Fast Forward. Published on July 25, 2016 as DOI: 10.1124/mol.116.104919
This article has not been copyedited and formatted. The final version may differ from this version.

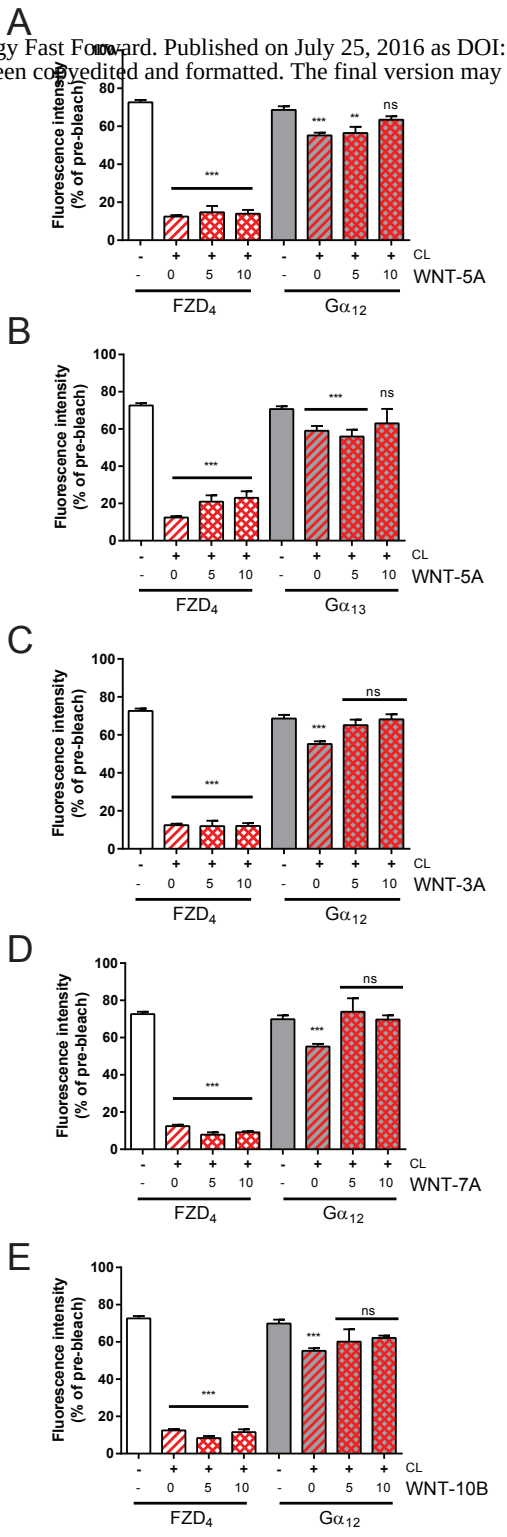

Fig. 3

Molecular Pharmacology Fast Forward. Published on July 25, 2016 as DOI: 10.1124/mol.116.104919
This article has not been copyedited and formatted. The final version may differ from this version.

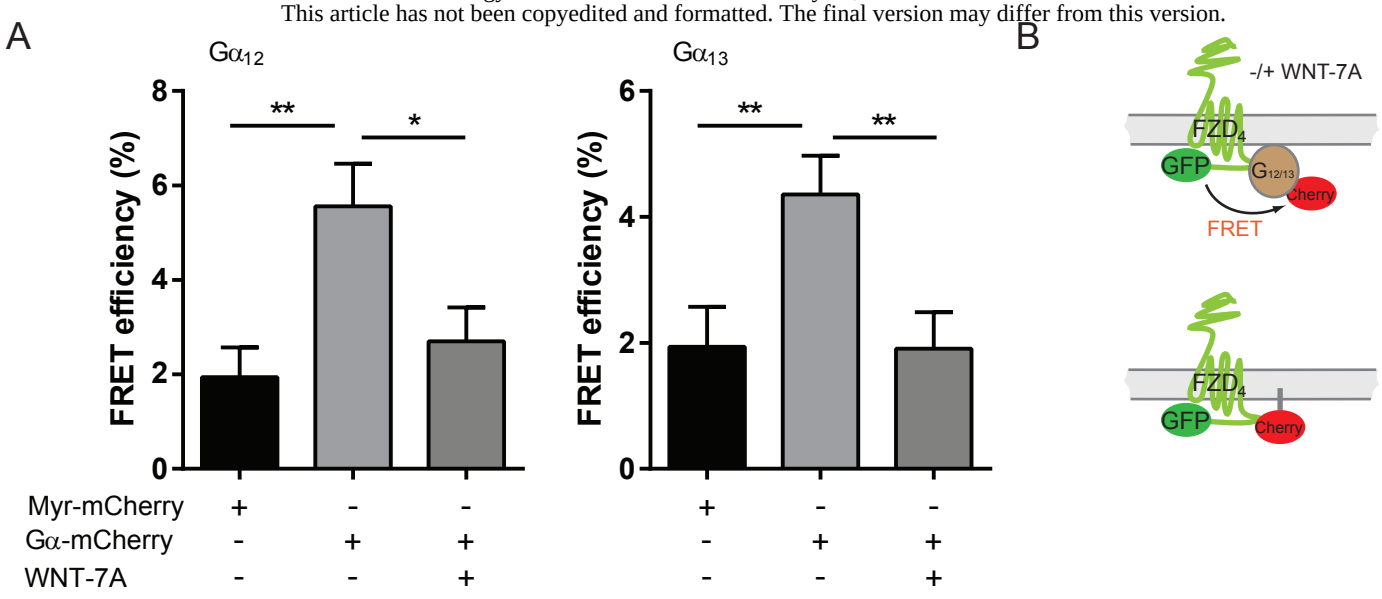

Fig. 4

Molecular Pharmacology Fast Forward. Published on July 25, 2016 as DOI: 10.1124/mol.116.104919
This article has not been copyedited and formatted. The final version may differ from this version.

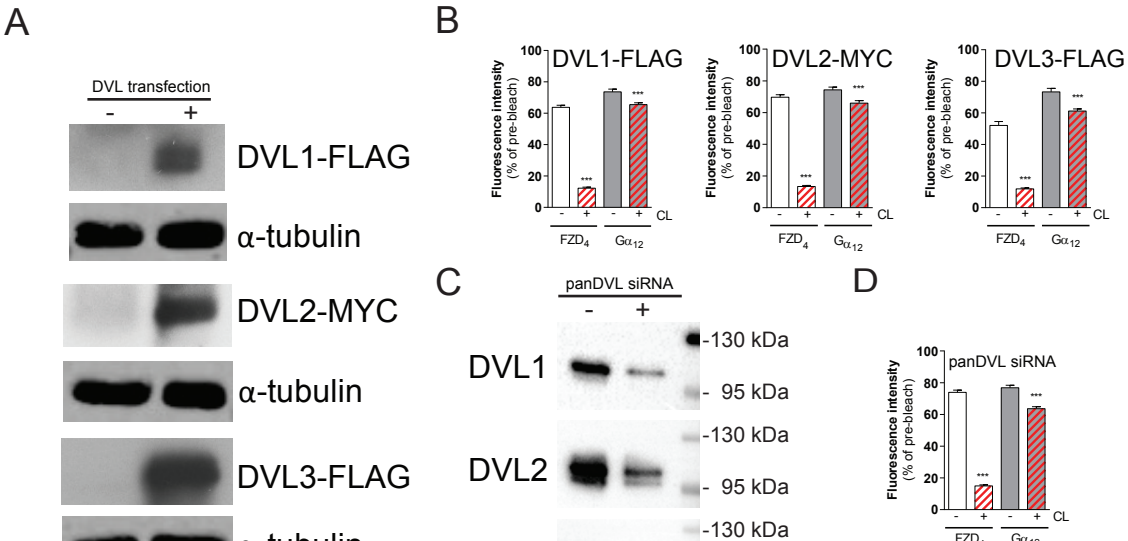

Fig. 5

Molecular Pharmacology Fast Forward. Published on July 25, 2016 as DOI: 10.1124/mol.116.104919
This article has not been copyedited and formatted. The final version may differ from this version.

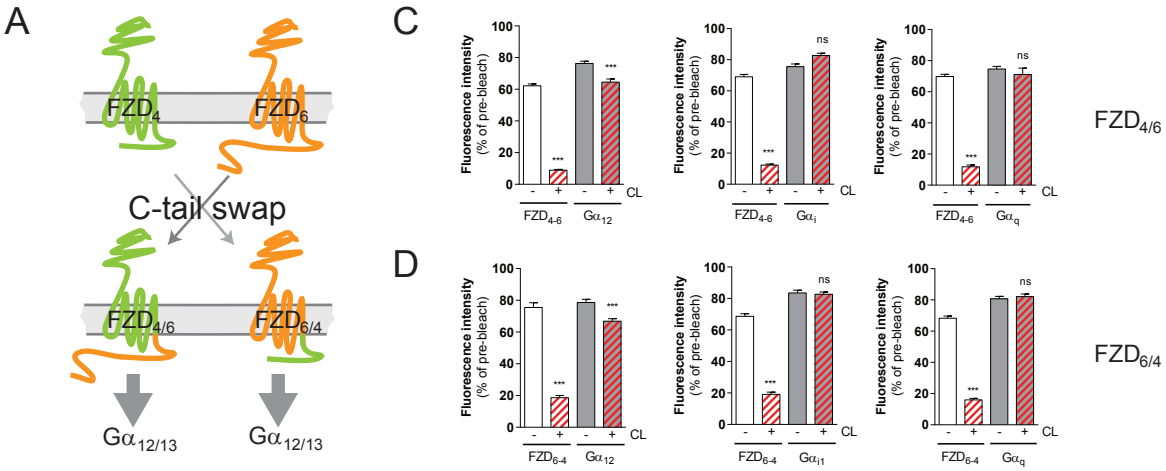

B

```
hFZD4 C terminus> SAKTLHTWQKCSNR.....................LVNSGKVKREKRGNG.................WVKPGKGSETVV
HFZD6 C terminus> SKKTCTEWAGFFKRNRKRDPISESRRVLQESCEFFLKHNSKVKHKKKHYKPSSHKLKVISKSMGTSTGATANHGTSAVAITSHDYLGQ
                    ETLTEIQTSPETSMREVKADGASTPRLREQDCGEPASPAASISRLSGEQVDGKGQAGSVSESARSEGRISPKSDITDTGLAQSNNL
                    QVPSSSEPSSLKGSTSLLVHPVSGVRKEQGGGCHSDT
```

Fig. 6

Molecular Pharmacology Fast Forward. Published on July 25, 2016 as DOI: 10.1124/mol.116.104919
This article has not been copyedited and formatted. The final version may differ from this version.

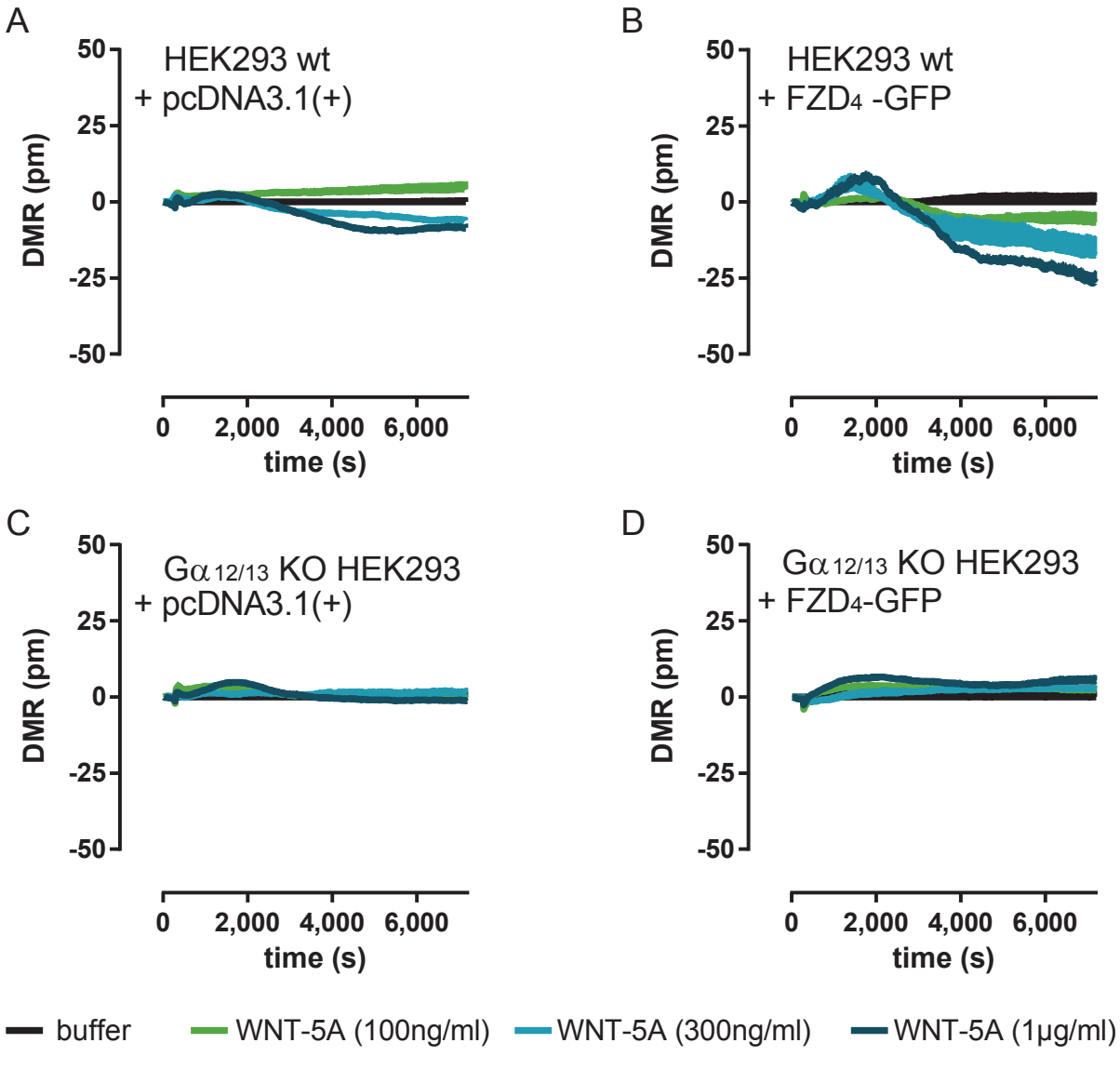

Fig. 7

Molecular Pharmacology Fast Forward. Published on July 25, 2016 as DOI: 10.1124/mol.116.104919
This article has not been copyedited and formatted. The final version may differ from this version.

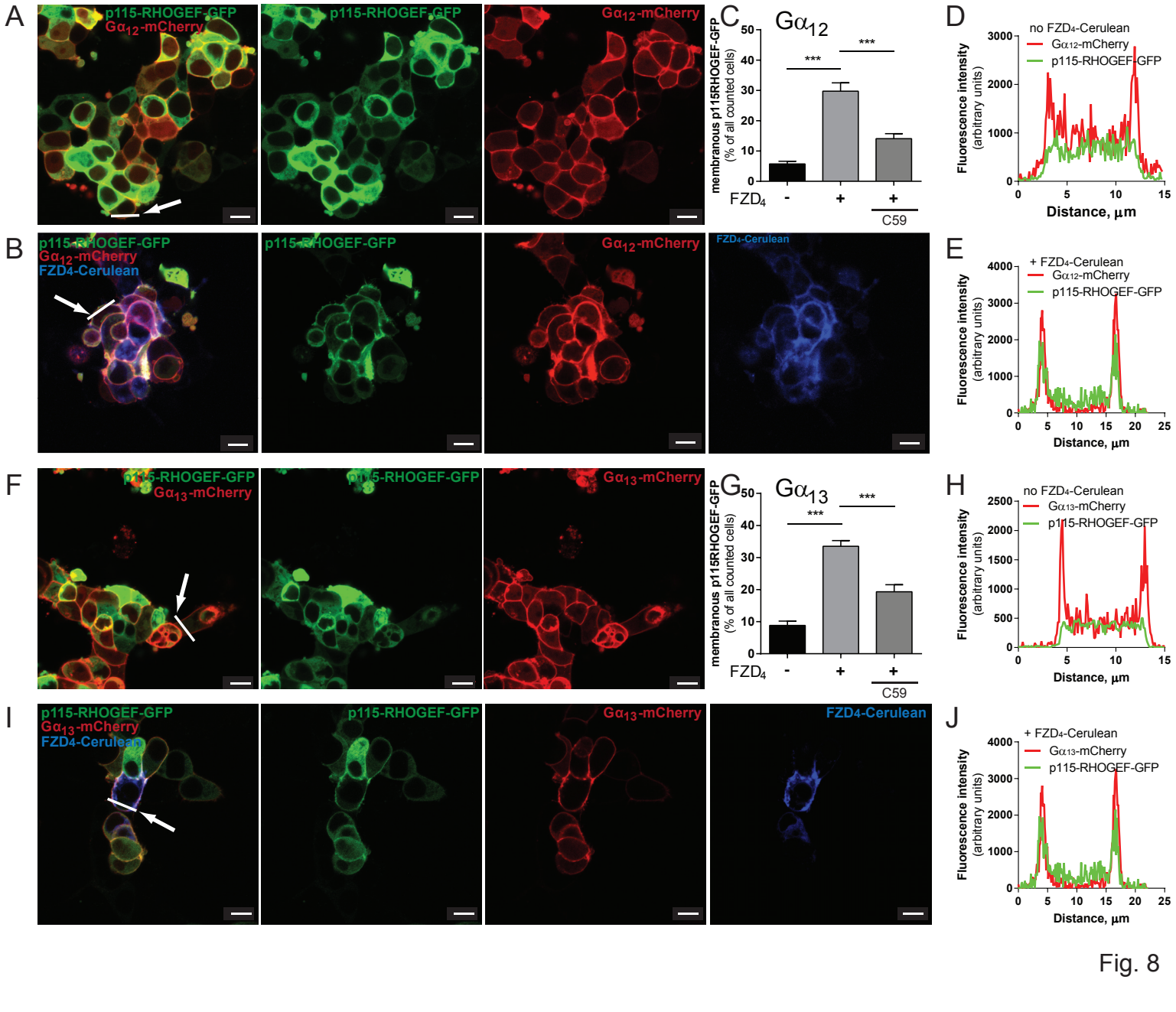

Fig. 8

Molecular Pharmacology Fast Forward. Published on July 25, 2016 as DOI: 10.1124/mol.116.104919
This article has not been copyedited and formatted. The final version may differ from this version.

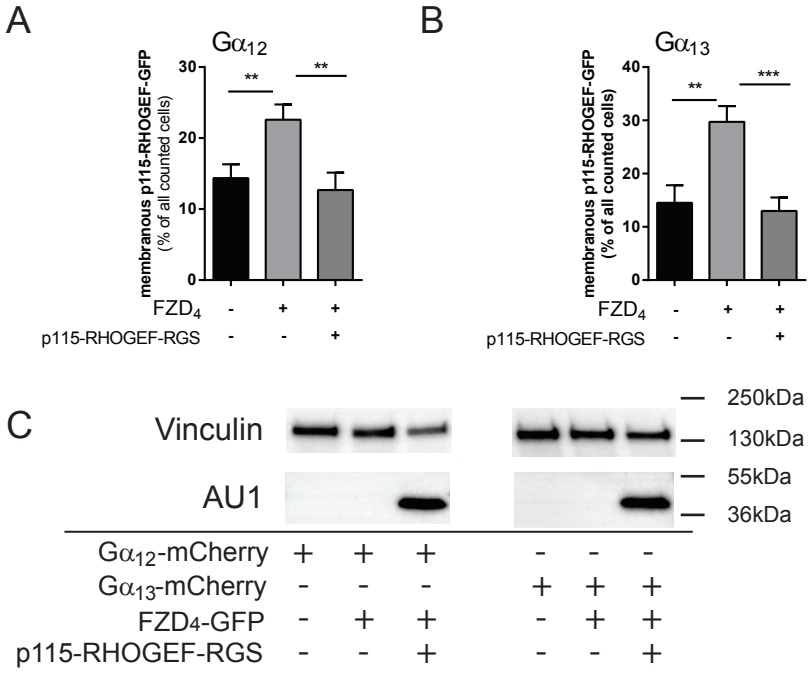

Fig. 9

Supplemental Data

WNT stimulation dissociates a Frizzled 4 inactive state complex with $G\alpha_{12/13}$

Elisa Arthofer, Belma Hot, Julian Petersen, Katerina Strakova, Stefan Jäger, Manuel Grundmann, Evi Kostenis, J. Silvio Gutkind, Gunnar Schulte

Section of Receptor Biology & Signaling, Dept. Physiology & Pharmacology, Karolinska Institutet, S-17177, Stockholm, Sweden (EA, BH, JP, KS, SJ, GS)

Section on Molecular Signal Transduction Eunice Kennedy Shriver National Institute of Child Health and Human Development, National Institutes of Health, 35A Convent Drive, MSC 3752 Bethesda, MD 20892-3752, USA. (EA)

Faculty of Science, Institute of Experimental Biology, Masaryk University, Brno, Czech Republic (KS, GS)

Molecular-, Cellular- and Pharmacobiology Section, Institute for Pharmaceutical Biology, University of Bonn, 53115 Bonn, Germany (MG, EK)

University of California San Diego, Dept. Pharmacology, Moores Cancer Center, 9500 Gilman Dr., La Jolla, CA 92093-0636, USA (JSG)

Table of contents

Supplemental Figure 1: Functional validation of C terminally-tagged FZD_4-GFP, FZD_4-mCherry and FZD_4-Cerulean in comparison to untagged FZD_4 by DVL recruitment. HEK293 cells were transfected with DVL1-FLAG alone (**A, B**) or in combination with human FZD_4-untagged, FZD_4-GFP, FZD_4-mCherry or FZD_4-Cerulean at a 3:1 DNA ratio receptor:DVL (**C-J**). After 24 h, cells were fixed in 4% PFA and stained by indirect immunocytochemistry with an anti-FLAG primary antibody and a Cy5-conjugated secondary antibody. Similar to what is known from other Class Frizzled receptors (Tauriello et al., 2012) and the C terminally tagged mouse FZD_4-GFP (Bryja et al., 2007), the C terminally-tagged versions of human FZD_4 used in this study efficiently recruited DVL1-FLAG from intracellular aggregates (see punctate pattern of DVL1-FLAG in absence of FZD coexpression) to a clear membrane localization. Since the C terminal KTxxxW sequence and the flanking regions of the third intracellular loop are involved in FZD-mediated DVL recruitment (Tauriello et al., 2012), this assay validates both membrane integration and functionality of the engineered human FZD_4. The white square marks the magnified area shown in the single-channel images. Size bars 20 µm. The ZEN2013 software was used to generate intensity profiles of the present fluorophores along a line passing through a single cell (**B, D, F, H, J**) . Profiles were created spanning from membrane to membrane crossing the cytosol but excluding the nucleus (white line across cell). The experiments were done three times and the results are summarized in the bar graph in (**K**). Between 12 and 296 cells per condition and independent experiment were counted by an observer blinded to the experimental condition Data are presented as mean±SEM. *** $p<0.001$ (all columns compared to control without FZD_4 expression). For figure see next page.

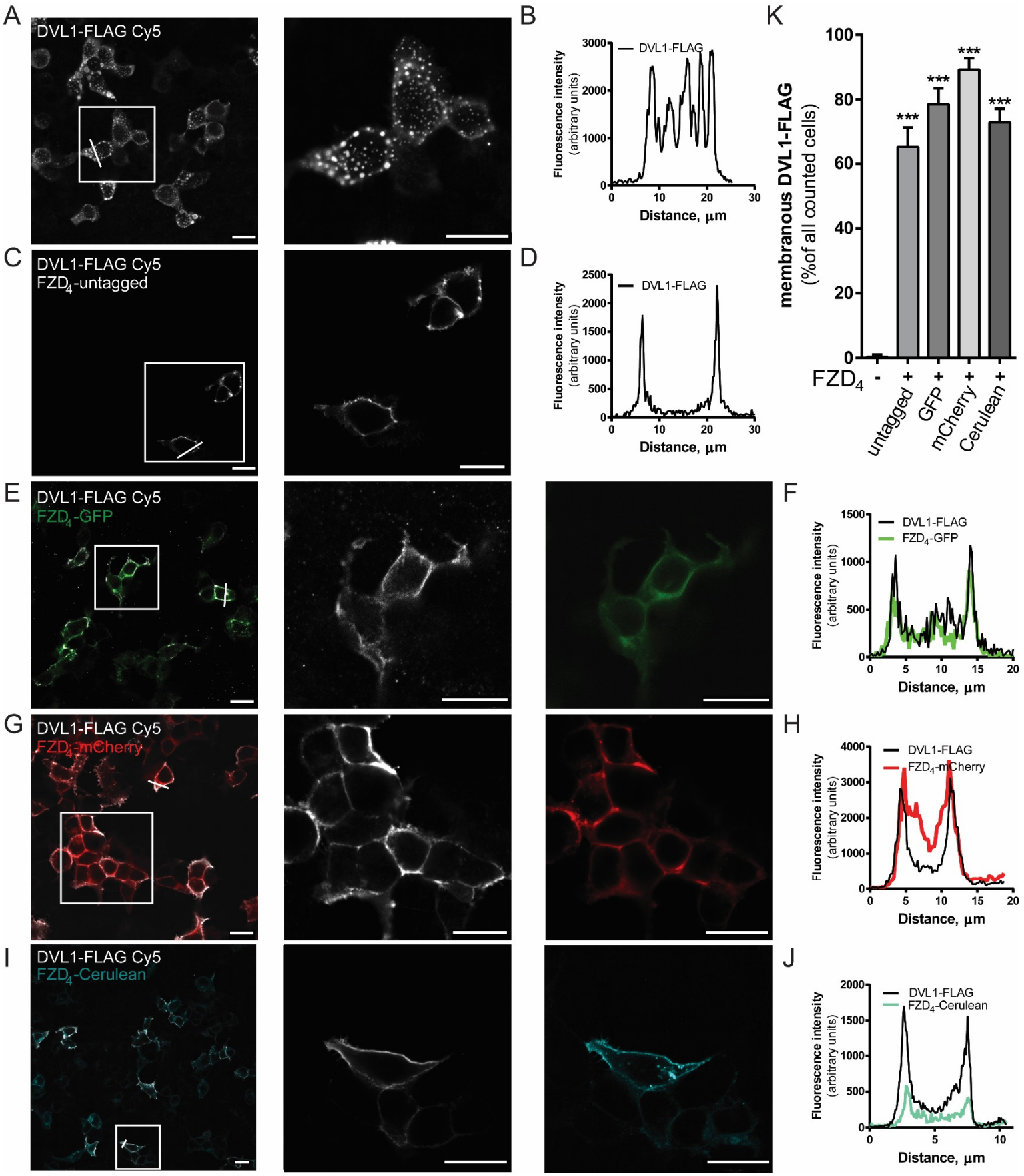
A
DVL1-FLAG Cy5
B
DVL1-FLAG
Fluorescence intensity (arbitrary units)
Distance, µm
K
membranous DVL1-FLAG (%of all counted cells)
FZD4 - + + + +
untagged
GFP
mCherry
Cerulean
C
DVL1-FLAG Cy5
FZD4-untagged
D
DVL1-FLAG
E
DVL1-FLAG Cy5
FZD4-GFP
F
DVL1-FLAG
FZD4-GFP
G
DVL1-FLAG Cy5
FZD4-mCherry
H
DVL1-FLAG
FZD4-mCherry
I
DVL1-FLAG Cy5
FZD4-Cerulean
J
DVL1-FLAG
FZD4-Cerulean

Supplemental Figure 2: Functional validation of N terminally-tagged $G\alpha_{12}$-mCherry employing p115-RHOGEF recruitment. HEK293 cells were expressed with p115-RHOGEF-GFP, LPA_1 receptor (untagged), and N terminally-tagged $G\alpha_{12/13}$-mCherry either alone or in combination (indicated in the figure). In all conditions, untagged $\beta\gamma$ subunits were coexpressed. p115-RHOGEF-GFP shows an even cytosolic distribution, which is not affected by cotransfection with LPA_1 receptor or with $G\alpha_{12}$-mCherry. However, the combination of $G\alpha_{12}$-mCherry and LPA_1 receptor induced a strong recruitment of p115-RHOGEF-GFP to the membrane-localized $G\alpha_{12}$-mCherry. Both the strict membrane localization and the effective p115-RHOGEF-GFP membrane recruitment underline that correct processing and functionality of the N terminally-tagged $G\alpha_{12}$-mCherry used in this study. The white square marks the magnified area shown in the single-channel images. Size bars 20 µm. N=3. Data quantification is presented in Supplemental Figure 4A. The ZEN2013 software was used to generate intensity profiles of the present fluorophores along a line passing through a single cell (white line across cell).

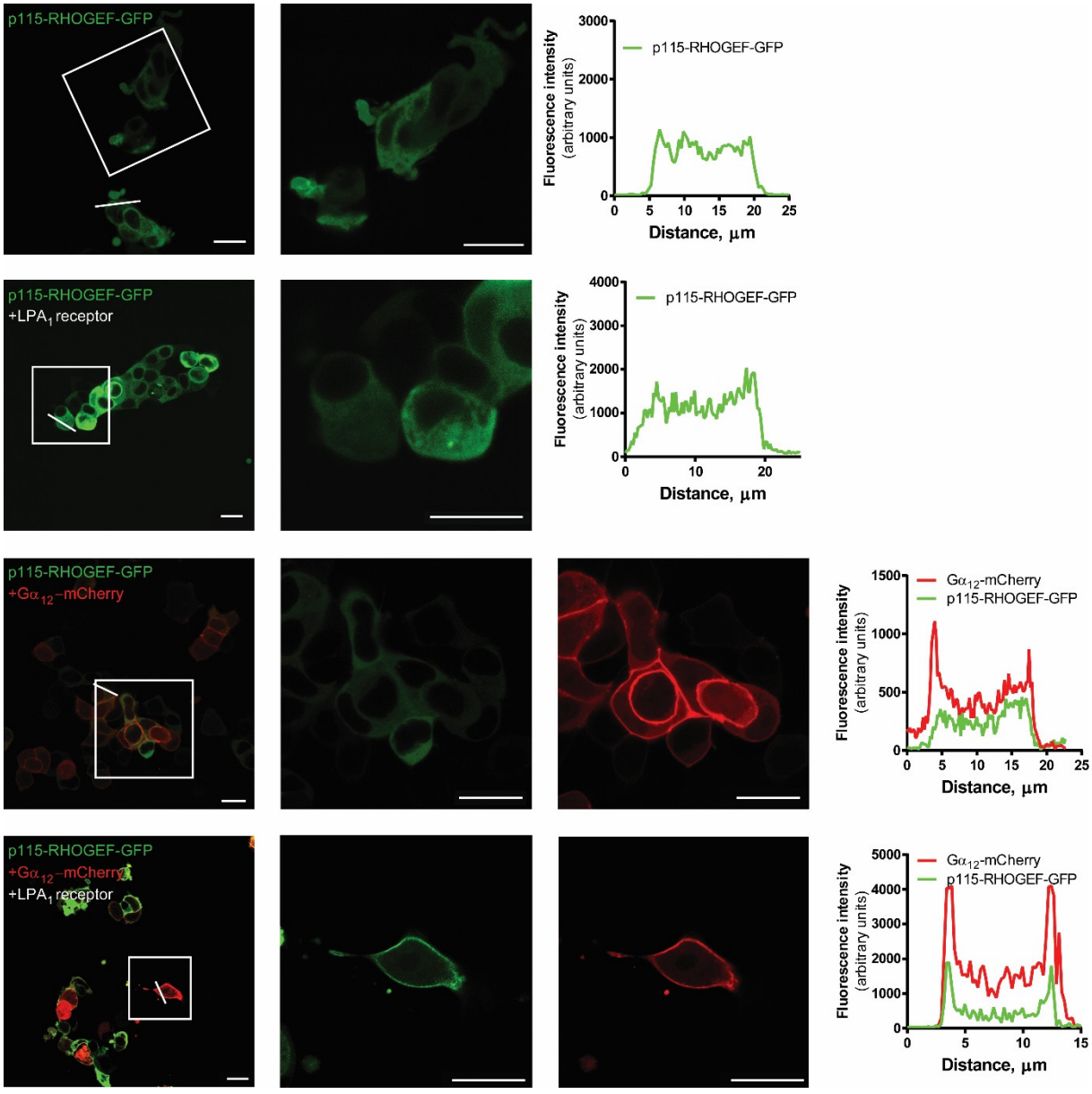

Supplemental Figure 3: Functional validation of N terminally-tagged Gα$_{13}$-mCherry employing p115-RHOGEF recruitment. HEK293 cells were expressed with p115-RHOGEF-GFP, LPA$_1$ receptor (untagged), and N terminally-tagged Gα$_{13}$-mCherry. In all conditions, untagged βγ subunits were coexpressed. p115-RHOGEF-GFP shows an even cytosolic distribution, which is not affected by cotransfection with LPA$_1$ receptor or with Gα$_{13}$-mCherry (see Supplemental Figure 2). However, the combination of Gα$_{13}$-mCherry and LPA$_1$ receptor induced a strong recruitment of p115-RHOGEF-GFP to the membrane-localized Gα$_{13}$-mCherry. Both the strict membrane localization and the effective p115-RHOGEF-GFP membrane recruitment underline that correct processing and functionality of the N terminally-tagged Gα$_{13}$-mCherry used in this study. The white square marks the magnified area shown in the single-channel images. Size bars 20 µm. N=3. Data quantification is presented in Supplemental Figure 4B. The ZEN2013 software was used to generate intensity profiles of the present fluorophores along a line passing through a single cell (see arrow).

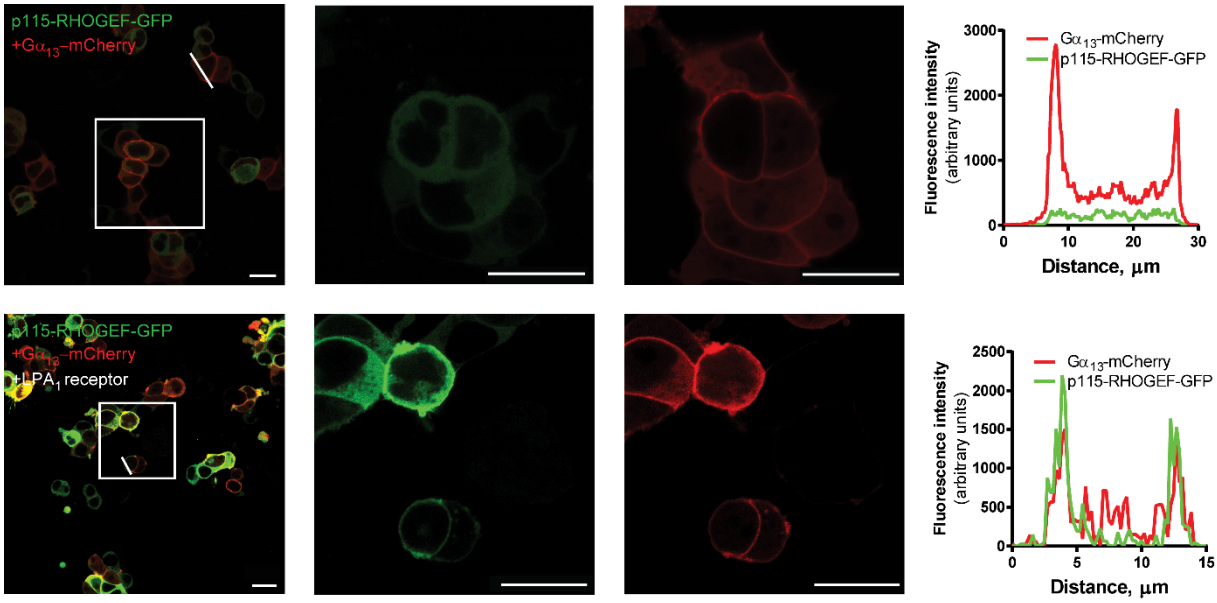

Supplemental Figure 4: Quantification of LPA_1 receptor-mediated p115-RHOGEF-GFP recruitment. Bar Graphs provide quantitation of the data presented in Supplemental Figure 2 and 3. HEK293 cells were transfected with p115-RHOGEF-GFP, LPA_1 receptor (untagged), either N terminally-tagged $G\alpha_{12}$ (**A**) or $G\alpha_{13}$-mCherry (**B**). In all conditions, untagged $\beta\gamma$ subunits were coexpressed. Cells were left either untreated or treated with 10 μM of the LPA_1R selective antagonist/inverse agonist Ki 16425. Data from 3 independent experiments are summarized in bar graphs (mean±SEM). More than 60 cells/condition and independent experiment were counted by a blinded observer. ** p<0.01; *** p<0.001.

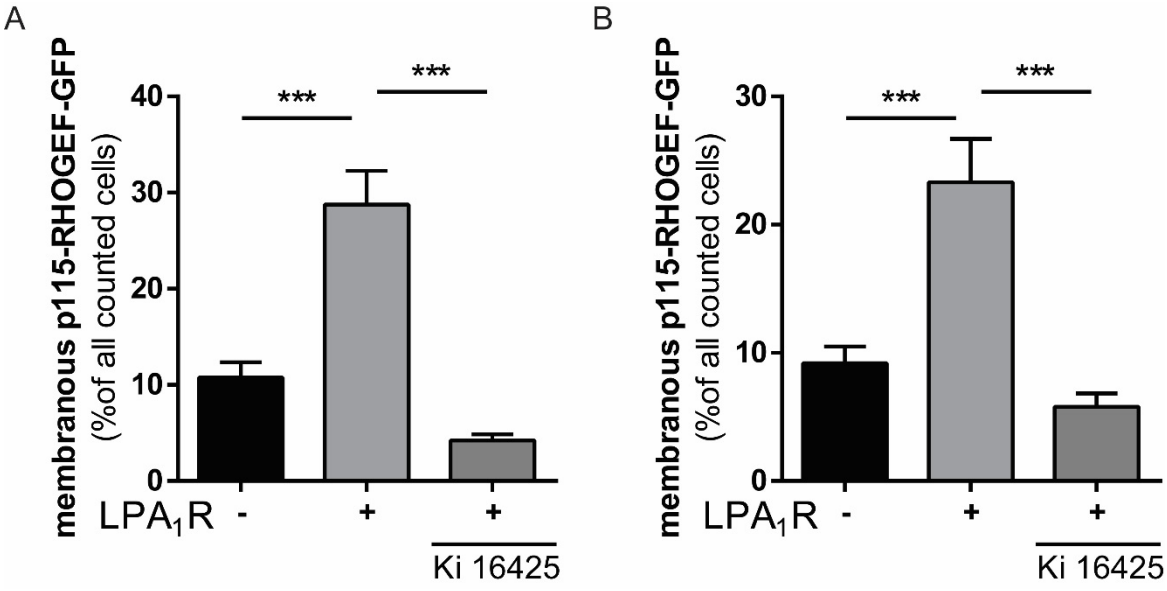

Supplemental Figure 5: Expression levels of FZD_4-GFP and forskolin-induced DMR responses in wt and $G\alpha_{12/13}$-knock out HEK293 cells. (**A-D**) Brightfield and GFP channel images of HEK293 wild-type (**A,B**) or $G\alpha_{12/13}$ KO HEK293 cells (**C,D**) transfected with pcDNA3.1(+) or FZD_4-GFP. Scale bar indicates 100µm. (**E**) Quantification of FZD_4-GFP expression by measuring fluorescence intensity of GFP-tagged receptor constructs. (**F,G**) Forskolin (fsk)-induced DMR response of HEK293 wild-type (**F**) and $G\alpha_{12/13}$ KO HEK293 cells (**G**) either transfected with empty vector or FZD_4-GFP. Shown are representative traces, buffer corrected and measured in triplicates +SEM.

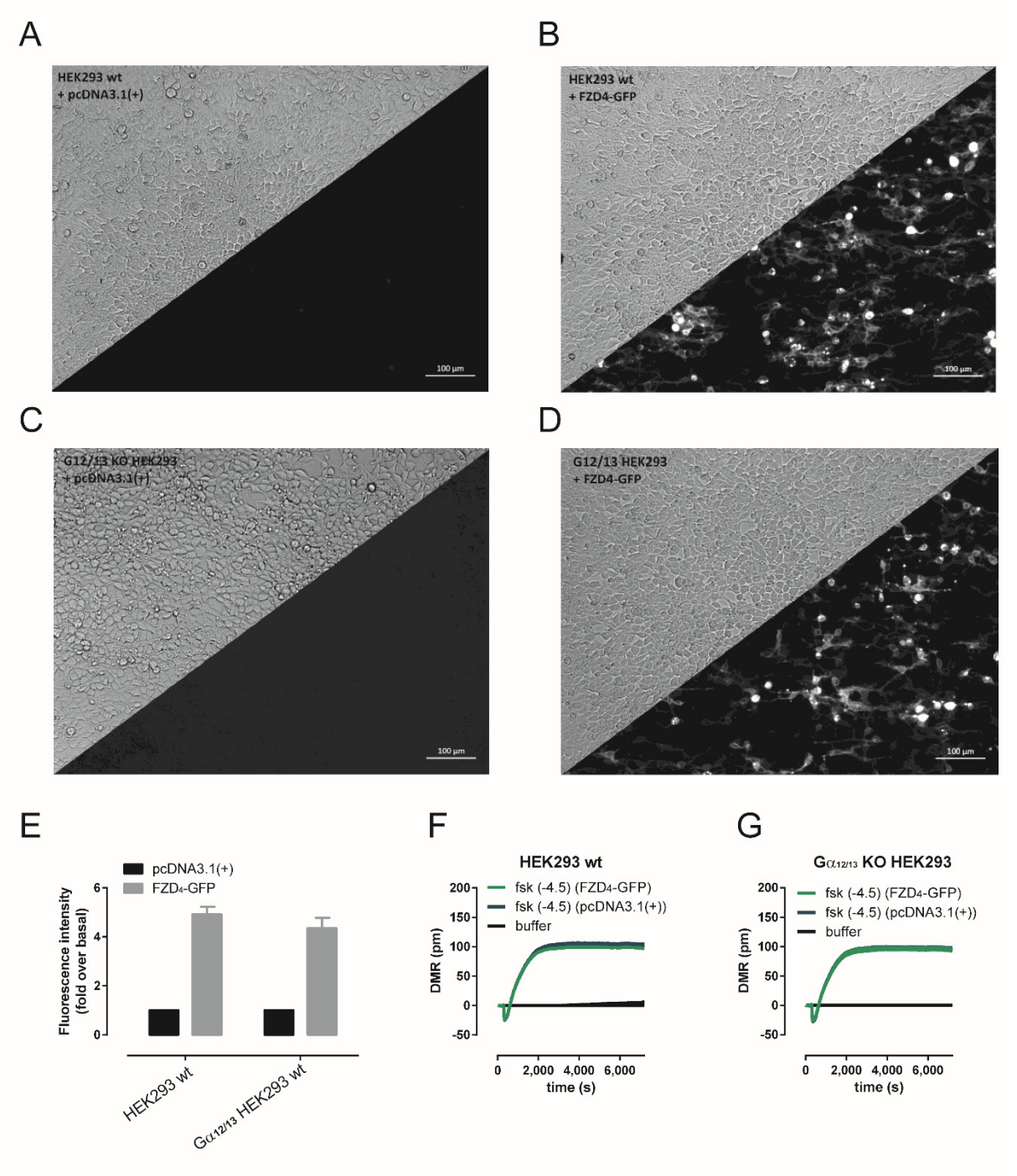

Supplemental Figure 6: Expression levels of DVL1, 2, 3 in HEK293 cells treated with ctrl and panDVL siRNA. The bar graph summarizes three independent experiments (corresponding to Fig. 5B), where DVL1, 2, 3 expression was quantified by densitometry of an immunoblot analysing cell lysates from ctrl siRNA and panDVL siRNA treated HEK293 cells. Endogenous levels of DVL1, 2, 3, were detected with anti-DVL1, 2 or 3 antibodies and quantified. DVL values were normalized to β-actin expression. Graph presents mean±SEM.

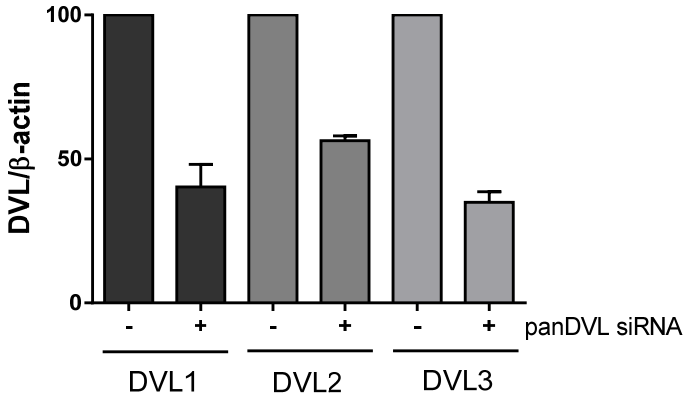

References

Bryja V, Gradl D, Schambony A, Arenas E and Schulte G (2007) beta-arrestin is a necessary component of Wnt/beta-catenin signaling in vitro and in vivo. *P Natl Acad Sci USA* **104**(16): 6690-6695.

Tauriello DV, Jordens I, Kirchner K, Slootstra JW, Kruitwagen T, Bouwman BA, Noutsou M, Rudiger SG, Schwamborn K, Schambony A and Maurice MM (2012) Wnt/beta-catenin signaling requires interaction of the Dishevelled DEP domain and C terminus with a discontinuous motif in Frizzled. *Proc Natl Acad Sci U S A* **109**(14): E812-820.